JOURNAL OF MATERIALS SCIENCE 16 (1981) 2935–2961

Review
Growth and characterization of InGaAsP lattice-matched to InP

P. A. HOUSTON
Department of Electronic and Electrical Engineering, University of Sheffield, Mappin Street, Sheffield, UK

The development of InGaAsP lattice-matched to InP as a suitable material for a range of electronic devices is reviewed. Currently accepted values of fundamental material parameters such as lattice constant, energy band-gap and effective mass as a function of composition are presented. The various growth techniques are discussed with particular emphasis given to the liquid phase epitaxy (LPE) method which has emerged as the most popular. Details of the determination of the liquidus and solidus phase diagrams both theoretically and experimentally are given and a comparison of the two is carried out. The problems of doping control and lattice matching are discussed. The other less widely-used growth methods, vapour phase epitaxy (VPE) and molecular beam epitaxy (MBE), are also outlined. The development of optical sources (lasers and LED's) and photo-detectors for optical-fibre communication systems is presented with particular attention being paid to the device technology. The latest performance figures in this rapidly moving area are reviewed. Prospects for the use of this material in non-optical applications are discussed in terms of its transport properties and device technology for applications in microwaves and high-speed logic.

1. Introduction

Except for the GaAlAs–GaAs heterojunction system, the III–V semiconductor ternary alloys can suffer from severe problems associated with lattice mismatch when grown on binary substrates. Heterojunctions are useful in providing carrier and optical confinement due to band-gap differences for applications in opto-electronic devices. These devices, however, require a low interfacial state density which demands good lattice matching between the different materials. The addition of a fourth component to the alloy system allows the band-gap to be changed whilst maintaining a given lattice constant to match a particular binary substrate.

The most important quaternary system at present is $In_{1-x}Ga_xAs_yP_{1-y}$. Fig. 1 shows the variation of band-gap as a function of lattice constant for the four ternary compounds which border the quaternary system. Any point inside this boundary represents a given quaternary composition with a value of lattice constant and corresponding band-gap. The ternary line for GaAlAs has been included for comparison. To maintain a given lattice constant for the quaternary system a simultaneous variation of the Ga/In and As/P ratio is required. This condition is represented by a vertical line within the boundary. Both InP and GaAs are useful substrates for lattice-matched heterojunctions. The InP-based system covers a band-gap energy range of 0.75 to 1.35 eV (1.65 μm to 0.92 μm) while the GaAs system band-gap energy ranges from 1.42 to 1.9 eV (0.87 μm to 0.65 μm). As can be seen from Fig. 1, matching to GaAs results in a similar range of band-gap energies to that in the well-developed GaAlAs–GaAs heterojunction system. The usefulness of this substrate in optical systems is therefore rather limited. On the contrary, InGaAsP matched to InP covers a longer wavelength region and as a result the

0022–2461/81/112935–27$04.70/0

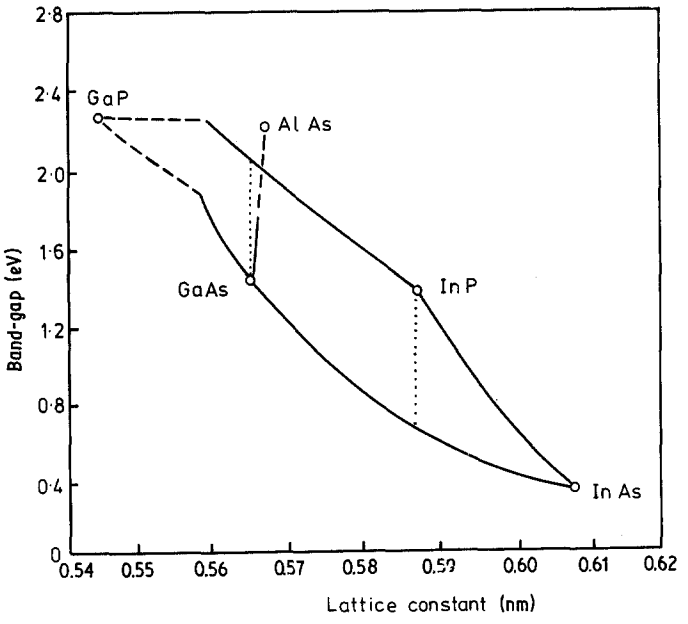

Figure 1 Band-gap energy for the InGaAsP quarternary system. – – – indirect gap; .... lattice-matched to InP or GaAs.

material has aroused great interest for sources in optical-fibre communications systems; in the 1.3 to 1.5 μm range, high-quality fused silica fibres exhibit minimum transmission loss and minimum material dispersion.

The rapid rise in development of the InGaAsP–InP system is due to some extent to "borrowed" growth and fabrication technology from the GaAlAs–GaAs heterojunction laser effort. In many ways however, the quaternary system has proved the easier system to grow and fabricate. Low growth temperatures (~650° C) ease problems associated with unwanted diffusion and substrate erosion. There are also fewer problems with oxide formation during and after growth. In addition, only two layers are required for a double heterostructure and ohmic contacts form more easily on InP than on either GaAs or GaAlAs. A counter to these advantages is the inevitable increased complexity of a four-component system. The transfer of liquidus information from laboratory to laboratory usually requires some fine adjustment in melt composition by a process of trial and error.

As well as the optical device applications for this quaternary system, interest has recently been expressed in the high-field transport properties for use in high-speed devices such as microwave FET's, transferred electron oscillators and high-speed logic. This aspect of InGaAsP has received much less attention except in the last few years and it is perhaps in this area that most has yet to be learned about this quaternary system.

The purpose of this review is to summarize the achievements in all areas of the growth and usage in InGaAsP lattice-matched to InP made over the last eight years. No such review exists at present and attempts are made to identify important areas of this quaternary system in which further work would be most valuable.

2. General properties

As already mentioned, the overriding advantage of using a quaternary material like InGaAsP is that independent control of energy gap over a wide range is possible for a given lattice constant. A three-dimensional representation of the direct energy-gap surface of this system is shown in Fig. 2. The iso-lattice constant sections are indicated which show the range of solid composition and corresponding band-gaps of the quaternary and ternary lattice-matched to InP and GaAs. It can be seen that band-gap energies can be covered almost continuously over the range 0.75 eV to 1.9 eV (1.65 μm to 0.65 μm) using GaAs and InP as substrates.

Assuming Vegard's law, the lattice constant, a, as a function of the composition parameters x and y can be written in terms of the lattice parameters of the four binaries, a_{GaAs}, a_{GaP}, a_{InAs} and a_{InP}, as

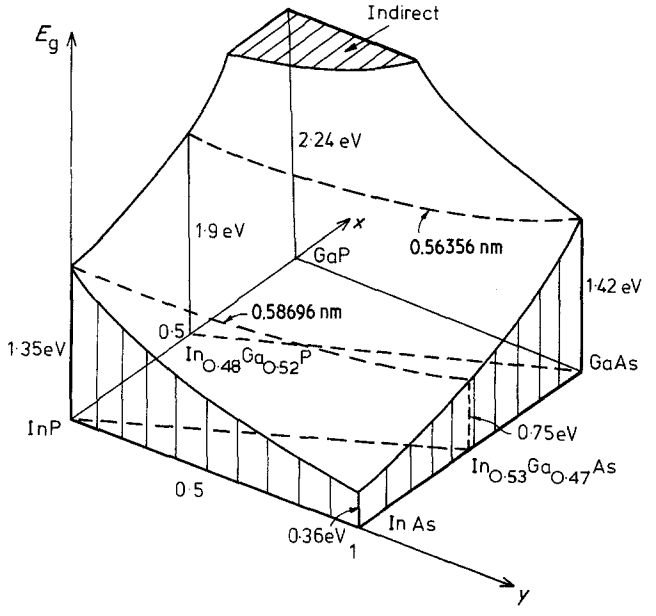

Figure 2 Direct energy band-gap surface for $In_{1-x}Ga_xAs_yP_{1-y}$ showing iso-lattice constant sections equivalent to InP and GaAs.

[1]

$$a(x,y) = xya_{GaAs} + x(1-y)a_{GaP} + (1-x)ya_{InAs} + (1-x)(1-y)a_{InP}. \quad (1)$$

Using quoted values for the binary lattice constants [1], and imposing a further condition of $y \simeq 2.2x$ for lattice matching to InP, Equation 1 becomes

$$a(y) = 0.58696 - 0.00008y + 0.00059y^2, \quad (2)$$

where a is measured in nm. The above two equations have been shown to agree well with experimental observations provided corrections due to strain are included.

A fundamental property of the InGaAsP system of great interest for optical applications is the band-gap energy, shown diagrammatically in Figs 1 and 2. Contrary to the case of lattice constant, in III–V ternary systems the band-gap as a function of composition is non-linear and can be described by a quadratic in the composition parameter. This means that the quaternary energy band-gap surface will be complex. The simplest relation, deduced by geometrical methods from the four ternary boundaries (see Moon *et al.* [2]) is given by [1]

$$E_g(x,y) = 1.35 + 0.668x - 1.17y + 0.758x^2 + 0.18y^2 - 0.69xy - 0.322x^2y + 0.03xy^2, \quad (3)$$

where E is measured in eV, which reduces to

$$E_g(y) = 1.35 - 0.867y + 0.334y^2 - 0.065y^2 \quad (4)$$

for quaternaries matched to InP ($y \simeq 2.2x$). However, this relation predicts too much bowing when compared to experimental measurements from photoluminescence [1, 3] and electroreflectance [4, 5] studies, as indicated in Fig. 3. The results of [1, 4, 5] are in very good agreement with each other and an empirical fit to the experimental points results in the relation [1].

$$E_g(y) = 1.35 - 0.72y + 0.12y^2, \quad (5)$$

where E_g is the band-gap energy, measured in eV, which is to be compared with the electroreflectance results of Yamazoe *et al.* [4] who give the coefficients of the second and third term in Equation 5 as -0.738 and 0.138, respectively. It has been concluded that the interpolation model of Moon *et al.* [2] is inadequate in explaining the detailed bowing effect in the band-gap surface.

The electron effective mass in $In_{1-x}Ga_xAs_yP_{1-y}$ is required for the prediction of transport properties in this material. Several measurements have been made on the quaternary lattice-matched to InP. Techniques which have been used are Shubnikov–de Haas resistance oscillations [7, 8], cyclotron resonance [6, 7, 9] and magnetophonon resonance [6, 7]. There was some discrepancy between the experimental results but the most recent publications [6, 8] have pointed out some

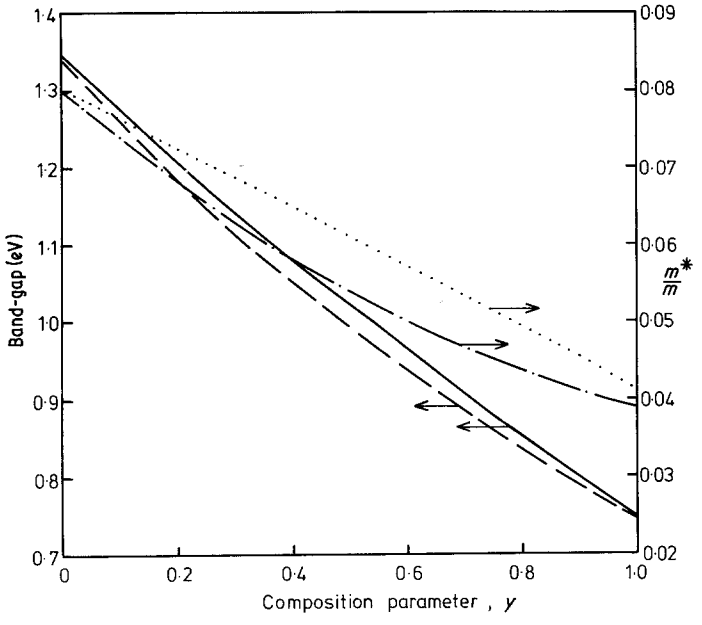

Figure 3 Band-gap and effective mass of InGaAsP lattice-matched to InP. – – – – calculated E_g [1]; ——— experimentally determined E_g [1, 4, 5]; .... experimentally determined m^*/m_0 [6]; – · – · – *k.p* theory m^*/m_0 [6].

errors in interpretation and the generally accepted values of effective mass, m^*, as a function of the composition parameter, y, is a linear relationship given by [6]

$$m^*/m_0 = 0.080 - 0.039y, \qquad (6)$$

where m_0 is the free electron mass, for quaternaries lattice-matched to InP (Fig. 3). The *k.p* perturbation theory has been used to predict effective masses in III–V alloys [10]. The theoretical *k.p* curve for InGaAsP lattice-matched to InP is included in Fig. 3, as outlined by Nicholas *et al.* [7] but using currently accepted band-gap energies [6]. An obvious discrepancy exists between the *k.p* theory and experiment which is thought to be due to the effects of alloy disorder.

3. Growth techniques

3.1. Liquid phase epitaxy

The first reported growth of lattice-matched InGaAsP on a binary substrate was made by Antypas *et al.* [11] in 1972. The method employed was liquid phase epitaxy (LPE) using the standard horizontal sliding graphite boat system (Fig. 4) in which they grew layers on InP substrates with a band-gap range from about 1 to 1.5 eV. LPE growth of III–V materials had previously been used extensively to produce a wide range of materials of extremely high quality. Briefly, the LPE growth technique involves the near equilibrium growth of a material from a saturated solution which is placed in contact with a polished substrate. In the case of III–V semiconductors the solvent is usually, but not necessarily, a Group III element with other Group III and Group V components dissolved in it to form a saturated solution at a chosen temperature. The temperature is lowered at a controlled rate just before or after contact has been made between the solution and the substrate. This induces supersaturation in the solution which causes the dissolved material to grow epitaxially onto the substrate. In a sliding graphite boat system growth is then terminated by sliding the solution off the substrate (Fig. 4) to remove all of the solution from the grown layer.

Several variations of the LPE growth theme are in use. A two-phase method employs a solid component in the solution to ensure exact saturation at all temperatures. Various cooling cycles are used such as isothermal step-cooling where the solution is cooled suddenly by several degrees before growth is initiated and a variation of this where cooling continues after growth is started. A problem with using InP as a substrate is the high vapour pressure of P over this binary which can result in thermal erosion before growth. Steps taken to minimize this effect include covering the substrate with InP during exposure to elevated temperatures and removing the damaged layer using an *in situ* etch back (undersaturated solution). The growth can be extended to include several successive

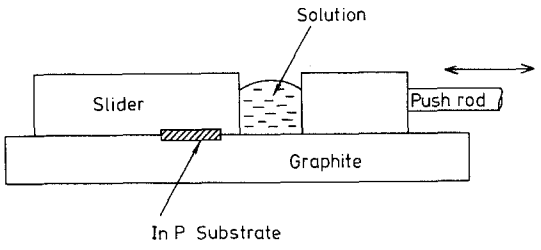

Figure 4 Schematic illustration of the sliding graphite boat system for LPE growth.

layers, each one from a different solution in a multi-well boat.

Obviously a knowledge of the liquidus curves is important to be able to prepare saturated solutions in the correct proportions in order to grow a required composition.

3.1.1 Experimental liquidus determination

The complexity of the phase diagrams of the quaternary systems means that they are much more difficult to determine either experimentally or theoretically than GaAs or InP. In the absence of the required thermodynamic data, the liquidus curves were determined experimentally [12–19] by first making up an undersaturated ternary solution of In + Ga + As. The solution is then equilibrated at the liquidus temperature and brought into contact with an InP seed. The P solubility is then obtained from the weight loss of the dissolved seed after a long period of contact with the solution. In, InAs and GaAs are usually used to provide the components of the ternary solution because of their ease of handling and weighing. A problem is evident here since, in the strict thermodynamic sense, only a solid quaternary can be in equilibrium with a quaternary solution. Experimentally, however, a type of equilibrium is observed when sufficient P has been incorporated into the In + Ga + As + P solution to saturate it. An interpretation of this effect was made by Ilegems and Pearson [20] in the GaAlAs system. These authors argued that a very thin layer of the solid ternary alloy, in equilibrium with the solution, was formed on the seed crystal thus preventing it from being further dissolved. In the system under review, a thin layer of InGaAsP of a composition in equilibrium with the solution protects the InP from further dissolution. As pointed out by Nakajima *et al.* [3] this layer will have to be removed from the seed to enable accurate weight-loss measurements to be taken. An alternative method is to observe the dissolution of known weights of the components in a solution [21] to determine the liquidus temperature. This method has been used in our laboratories by making use of direct observation of the solution in a "see-through" gold-plated furnace. The technique involves heating up the solution to several degrees past the point at which all of the carefully weighed components are dissolved to ensure that the solution is completely homogeneous. The temperature is dropped until a solid forms and then raised again very slowly while observing the point at which complete dissolution occurs. Slight tapping of the furnace helps to ensure dissolution under equilibrium conditions. The use of two-phase solution growth [17] eliminates the need to control exactly the amount of P required by adding excess InP to the In + Ga + As solution. An additional benefit from this method is that automatic saturation of the solution is maintained throughout a range of temperature excursions. Possible disadvantages are that the amount of supersaturation is difficult to control and that growth-rate reproducibility might suffer due to competition for the growth between the substrate and the irregularly-shaped solid pieces.

The results of the experimental liquidus determination for the In-rich InGaAsP system have led to the production of much data [3, 12–17] over a whole range of liquid compositions and temperatures. However, we are most interested in compositions which exhibit lattice-matching to InP. The main conclusion which can be drawn from the data is that the addition of Ga to the quaternary melt results in an appreciable decrease in the solubility of P while the presence of As has a much less pronounced effect [3, 12]. Nakajima *et al.* [3] have shown that reasonable agreement on the liquidus determination has been obtained by several authors. Fig. 5 shows a curve which indicates the liquidus compositions of As and P as a function of Ga composition. Fig. 6 shows the corresponding x and y values ($In_{1-x}Ga_xAs_yP_{1-y}$). Both Figs 5 and 6 refer to lattice matching to InP substrates at a growth temperature of about 650° C. There is fair agreement between the different authors and these curves would serve as a starting point for workers without their own data. However, to obtain good lattice matching it is necessary to carry out some "fine adjustments" to the solution compositions.

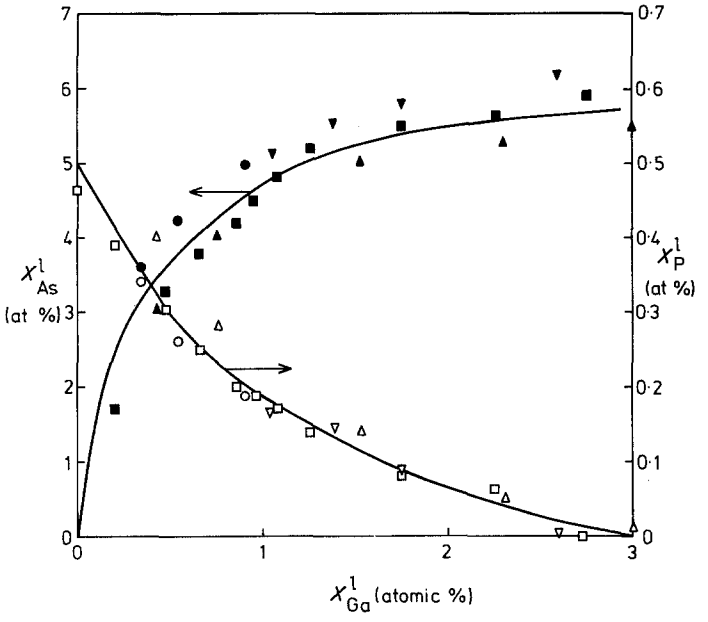

Figure 5 Liquidus composition curves for In + Ga + As + P solutions used in the growth of quaternaries lattice-matched to InP at a growth temperature of approximately 650° C. (1 0 0): X^l_{As}, ● and X^l_P, ○ [16]; (1 0 0): X^l_{As}, ■ and X^l_P, □ [17]; (1 0 0): X^l_{As}, ▲ and X^l_P, △ [3]; (1 1 1)B: X^l_{As}, ▼ and X^l_P, ▽ [18] (1 0 0) and (1 1 1).

The majority of workers in the early stages of experimental determination of the liquidus curves studied growth on (111)-orientated InP substrates [3, 12–15]. There are important advantages however in using (100) orientation because of the cleaving and preferential etching properties of III–V compounds. Hsieh *et al.* [21] reported different InGaAsP solid compositions when grown on (100) and (111)B InP substrates using the same solution composition. Antypas and Shen [22] found that the incorporation rate of Ga and As is different for (111)A and (111)B orientations of InP. Oe and Sugiyama [23] made a comparison of liquidus determinations using both (100) and (111)B InP substrates to saturate the solution and obtained different results. They also carried out growth on both substrate orientations using the solutions which were saturated from the corresponding orientated substrates and found that, in addition, the quaternary growth developed at a much slower rate on the (111)B orientation substrate. The solid compositions which lattice-matched to InP for the two different orientations were also different. The effects of the different orientations used in Fig. 5 do not show up easily due to the scatter in the experimental points. These orientation effects correspond to differences of 2 to 3°C in the liquidus temperature and must be taken into account when using the same growth conditions on differently orientated substrates. The question is also raised as to the advisability of using multi-orientated InP pieces, polycrystalline source substrates and single-crystal sources of different orientation to the seed crystal, in two-phase growth.

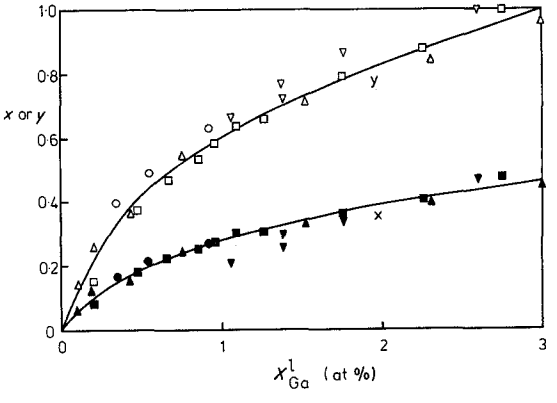

Figure 6 The solidus parameters x and y corresponding to the data of Fig. 5. x: ●, y: ○ [16]; x: ■, y: □ [17]; x: ▲, y: △ [3]; x: ▼, y: ▽ [18].

The ternary $In_{0.53}Ga_{0.47}As$, which is lattice-matched to InP, has become important as a competitor to Ge for use in photodetectors at 1.6 μm [24] and also as a potential material for high-speed applications. Because of these applications, particular attention has been paid to establishing the phase diagrams and growth condition [25–34] for $In_{1-x}Ga_xAs$ and, in particular, the composition which is lattice-matched to InP ($x = 0.47$). Nakajima *et al.* [34] have used a method of monitoring the liquidus of the ternary by making use of an InP seed to check for saturation of In + Ga +

TABLE I Parameters for growth of $In_{0.53}Ga_{0.47}As$ on InP

Substrate orientation	Growth Temperature (°C)	X^l_{Ga} (at%)	X^l_{As} (at%)	Reference number
(100)	650	2.45	5.96	[34]
(100)	621	2.1	4.7	[30]
(100)	650	2.6	6.2	[18]
(100)	635	2.75	5.9	[17]
(100)	650	3.1	5.53	[3]
(100)	632	2.2	5.1	[33]
(111)B	650	3.1	5.5	[34]
(111)B	650	3.06	5.59	[27]
(111)B	~625	2.75	4.6	[35]
(111)B	650	3.8	5.0	[36]
(111)B	645	3.6	5.8	[37]
(111)B	617	2.6	4.3	[38]

As solution. No loss of P indicates a saturated solution. This method overcomes problems of excess growth on InAs or GaAs seeds after removal from the solution. A summary of the liquidus compositions for $In_{0.53}Ga_{0.47}As$ obtained by several workers is contained in Table I. An orientation dependence of the Ga incorporation into the ternary solid has been observed [31, 34] similar to that observed in the quaternary. Antypas *et al.* [31] have reported this dependence as a function of temperature by a (thermally-activated) Arrhenius relationship where the activation energies for (100) and (111)B substrates are different. They found a cross-over point at 629°C where the Ga incorporations for both orientations are equal. It is likely that similar cross-over points exist in InGaAsP. These observations indicate that nucleation depends critically on the surface energy of formation of the epitaxial layer. A consequence of this is that preparation of substrate surfaces is critically important (as with all epitaxy) in determining growth conditions and may well be an overriding factor which adds yet another source of variation in growth conditions from laboratory to laboratory.

3.1.2. Phase diagram calculations

The theoretical prediction of quaternary phase diagrams is an obvious requirement for ease of setting-up LPE growth conditions since experimental determination of liquidus data can be tedious. The complex thermodynamic processes which dictate the form of the phase diagrams for InGaAsP have been described with the aid of various simplified models. Even these models require lengthy descriptions with much involved algebraic manipulation. Here only the important points regarding the theoretical prediction of phase diagrams will be discussed and the usefulness of various values of thermodynamic quantities will be compared.

The free energy per mole, G, of a quaternary solid in equilibrium with a quaternary liquid is given by [39]

$$G = 2\sum_{i=1}^{4} N_i^s \mu_i^s = 2\sum_{i=1}^{4} N_i^l \mu_i^l, \tag{7}$$

where N_i^s and N_i^l are the atom fractions of component i in the solid and liquid, respectively, and μ_i^s and μ_i^l are the chemical potentials in the solid and liquid, respectively. The factor 2 in the summation converts notation from g atom^{-1} to g mol^{-1}. The solid–liquid equilibrium criterion used in Equations 7 is that

$$\mu_i^s = \mu_i^l \tag{8}$$

at constant temperature and pressure.

In an ideal solution in the interchange energies between different components are zero.

In this case

$$\mu_i^l = \mu_i^{0l} + RT\ln N_i^l, \tag{9}$$

where μ_i^{0l} is the standard chemical potential of component i in the liquid phase, T is the absolute temperature and R is the gas constant. In the regular solution model only interactions between neighbouring components are considered important and the interchange energies are non-zero. In this case the chemical potential becomes

$$\mu_i^l = \mu_i^{0l} + RT\ln a_i^l, \tag{10}$$

where a_i is called the activity of component i and can be written

$$a_i = \gamma_i N_i, \tag{11}$$

where γ_i is the activity coefficient and takes account for the non-ideality of the solution. The free energy of mixing, G_m, for a regular quaternary solution of n moles is now given by [40]

$$G_m = \frac{1}{2}\sum_{\substack{k=1\\k\neq j}}^{4}\sum_{j=1}^{4}\frac{\alpha_{kj}n_k n_j}{n} + RT\sum_{k=1}^{4} n_k \ln N_k, \tag{12}$$

where n_k and n_j are the number of moles of the 4 binary compounds and α_{kj} are the interchange energies or interaction parameters for the four binary liquid solutions and are related to the interaction energies of the nearest-neighbour pairs. Equations 12 show that, for the regular solution

model, G_m is composed of an ideal solution term (second term) plus a heat-of-mixing term (first term).

The solid–liquid phase equilibrium conditions for a regular liquid solution model and an ideal solid solution for the four binary compounds (GaAs, InAs, GaP and InP) are given by [14]

$$\ln(\gamma_{ij}^{s}N_{ij}^{s}) = \frac{\Delta S_{ij}^{F}(T_{ij}^{F}-T)}{RT+\ln(4\gamma_i^{l}\gamma_j^{l}N_i^{l}N_j/\gamma_i^{sl}\gamma_j^{sl})}, \quad (13)$$

where γ_{ij}^{s}, N_{ij}^{s}, ΔS_{ij}^{F}, and T_{ij}^{F} are the activity coefficient in the solid, the mole fraction in the solid, the entropy of fusion and the temperature of fusion of binary compounds ij; γ_i, γ_i^{sl} and N_i are the activity coefficient in the quaternary liquid, the activity coefficient in the stoichometric liquid and the atom fraction of element i in the quaternary liquid. For an ideal solid solution $\gamma_{ij}^{s}=1$. The activity coefficient of component i in a regular quaternary liquid solution is of the form [40]

$$RT\ln\gamma_i = \sum_{\substack{j=1\\ i\neq 1}}^{4}\alpha_{ij}N_j^{l^2} + \frac{1}{2}\sum_{\substack{k=1\\ k<j,\ i\neq k,\ i\neq j}}^{4}\sum_{j=1}^{4}N_k^{l}J_n^{l} \times(\alpha_{ij}+\alpha_{ik}-\alpha_{kj}). \quad (14)$$

From a knowledge of all the interaction parameters Equations 14 can be substituted into Equations 13 to solve for the liquidus temperature T and solidus composition N_{ij}^{s} for a given liquidus composition. Equations 14 apply equally well to the ternary and binary expressions for the activity coefficients with i, j and k all taking values not greater than 3 and 2 for the ternary and binary, respectively.

One of the earliest attempts at predicting the phase diagram of the InGaAs system was carried out by Wu and Pearson [25]. They considered a quasi-regular or simple solution approach where the interaction parameters took on values which were linear functions of temperature ($\alpha = a + bT$) rather than constant values for the strictly regular solution model. To obtain good agreement with experimentally-determined liquidus curves however, a curve-fitting technique was employed to determine "best-fit" values of α. Using these methods, Wu and Pearson were able to obtain very good agreement with experiment for both the liquidus and solidus in the temperature range 600 to 800° C in the indium-rich corner of the phase diagram. Stringfellow [41] has developed a model which is capable of predicting the interaction parameters for the solid from a knowledge only of the lattice parameters of the bounding III–V binary compounds. Using this model for the solid and the simple-solution model for the liquid he was able to calculate the InGaAsP phase diagram [42] using published thermodynamic parameters [43]. The agreement with experiment was poor but it was pointed out that in using this solid-solution model agreement was at least as good as that obtained for the ternaries using widely-accepted models. Antypas and Edgecumbe [14], using regular (simple) and ideal-solution models for the liquidus and solidus, respectively, also calculated the expected phase diagrams and obtained similar results for the liquid solutions to those of Stringfellow [42]. In both of these studies no attempt was made to adjust the parameters used in the calculation to fit the experimental data. Calculations were made of the distribution coefficients of P, Ga and As [14] and good agreement with experiment was obtained. These authors showed that for the temperature range 600 to 750° C the distribution coefficients varied significantly with temperatures for As and P but remained essentially constant for Ga. This has implications concerning layer composition grading if growth is carried out over large temperature excursions.

Further, more recent attempts have been made to predict the phase diagram of InGaAs [34, 38, 44] and InGaAsP [15, 45]. Most of the parameters used result from data collected on binary compounds at temperatures of 800° C or above and may not relate to the relatively low growth temperatures of the system of interest. This may be one of the reasons for poor agreement with experiment. Good curve fitting with experimental data nearly always involved adjustable interaction parameters [25, 34, 36, 38, 44, 45] and in two cases [25, 44] concentration-dependent interaction parameters have been employed to obtain agreement over the whole composition range. Whether the disagreement between theory and experiment is due to the inadequacy of the models for describing the thermodynamics of the system or due to the non-availability of the correct interaction parameters is at the moment unclear. A recent paper by Perea and Fonstad [46] has reported carefully-measured liquid interaction parameters for InP, InAs, GaAs and GaP in the

temperature range 580 to 670° C, relevant to InGaAsP growth on InP.

These values await application to the simple solution models to test agreement between these models and the experimentally-observed behaviour. In general, however, the models presented so far which attempt to describe the thermodynamic processes of the InGaAsP system are inevitably no better than the parameters which are fed into them and are not capable of predicting phase diagrams of unknown systems. The effect of substrate orientation on solidus data, as pointed out by Pearsall *et al.* [30], has not, up till now, been taken into account and may not be insignificant. Thus it seems that some more comprehensive model is required to predict phase diagrams of all III–V compounds including InGaAsP.

So far none of the theoretical models we have considered have indicated the possibility of a miscibility gap in the InGaAsP system. It is our experience, and that of some others, that often growth of the quaternary near the InGaAs end of the compositions lattice-matched to InP becomes more difficult. A very recent paper by de Cremoux *et al.* [47] has reported that when a previously derived expression for the solid composition as a function of growth temperature [48] (based on diffusion-limited growth) is combined with thermodynamic phase model calculations, a miscibility gap is predicted in this system. This shows up as calculated values of the differential distribution coefficients becoming infinite. That the experimental evidence seems on the whole to disagree with this finding is explained by de Cremoux *et al.* [47] in terms of the effect of lattice strain energy. When a lattice strain energy term [proportional to $(a-a_0)^2$] is included in the free energy expression, this energy contribution can become significant compared to the free energy of mixing for systems existing near a region of immiscibility [49]. In this case large lattice parameter changes can occur during small growth changes and minimizing strain energy can dictate the solid composition. This process, however, will only delay the onset of immiscibility and experimental evidence should be sought at low growth temperatures. An important implication of the possible closeness of the normal growth conditions of InGaAsP lattice-matched to InP to a miscibility gap may be the resultant effects on electron transport properties of the quaternary. This aspect will be discussed more fully in Section 5.1.

3.1.3. Lattice matching

The successful application of heterojunctions for optical sources (lasers and LED's) requires low carrier recombination velocities in order to avoid substantial non-radiative recombination due to interfacial states. This requirement implies the necessity of exactly lattice-matched heterojunctions. It can be seen from Figs 1 and 2 that both GaAs and InP are suitable binary substrate materials onto which lattice-matched layers of InGaAsP can be grown over a wide range of solid composition.

In addition to causing large interfacial state densities, lattice mismatch can seriously degrade the surface morphology of the grown layers. Hsieh *et al.* [21] have demonstrated that quaternary layers equivalent to wavelengths of 1.22 to 1.1 μm can be grown with a mismatch, $\Delta a/a$, given by

$$\frac{\Delta a}{a} = \frac{a_{\text{layer}} - a_{\text{InP}}}{a_{\text{InP}}} \tag{15}$$

of up to +0.4%, albeit with a certain number of cleavage steps. Feng *et al.* [50] have reported, however, that mismatch effects are far more sensitive to lattice mismatch for 1.31 μm material than for 1.15 μm material. For a given mismatch the surface morphology is poorer for the longer wavelength, resulting in melt removal problems unless the mismatch is less than 0.09%. Good quality crystals can only be grown over this range when less than 0.03% lattice mismatch is achieved. At the high-wavelength end of the InGaAsP system on InP, InGaAs shows severe cracking at −0.22% mismatch and prominent cross-hatch patterns occur at +0.28% [26]. The effects of solution supercooling on the lattice mismatch for the same liquid composition has been studied [21, 33] and little effect has been observed up to a supercooling of about 8° C in the case of (100)-oriented substrates; however, the effect is observed at lower values of supercooling for (111)B substrates [21].

Since the LPE growth of these compounds necessarily involves large temperature excursions the question of thermal expansion differences between quaternary and ternary layers and InP should be raised. Bisaro *et al.* [51] have measured the thermal expansion coefficient for InP, $In_{0.74}Ga_{0.26}As_{0.60}P_{0.40}$ and $In_{0.53}Ga_{0.47}As$ between the temperatures of 25 and 400° C and obtained values of

$$(4.56 \pm 0.10) \times 10^{-6}\,^{\circ}C^{-1},$$

$$(5.42 \pm 0.10) \times 10^{-6}\,^{\circ}C^{-1},$$

and

$$(5.66 \pm 0.10) \times 10^{-6}\,^{\circ}C^{-1},$$

respectively. The ternary and this particular composition of quaternary have values which are quite close. However, a substantial difference is observed between these values and InP, which means that a layer exactly lattice-matched at room temperature will be mismatched at the growth temperature by as much as +0.06%. A study of misfit dislocation of InGaAs on InP [52] has shown that dislocations are more easily generated at high temperatures. Dislocation-free epitaxial layers could only be grown when the lattice mismatch was between −0.65% and −0.09% at room temperature for a growth temperature of 650°C. This result is important for growing dislocation-free quaternary double-heterostructure lasers. The existence of mismatch has also been shown to affect the chemical transition widths at the heterojunction interfaces [53], as shown up by Auger profiling. Lattice mismatches of <0.03% gave sharp interfaces whereas substantial grading occurred at mismatches of −0.11% and +0.20%. The grading was larger for greater mismatch and also for InP grown on InGaAsP rather than InGaAsP on InP. This latter effect is most probably due to the lack of proper equilibrium of the InP solution with the quaternary solid and therefore the lesser tendency for growth under given conditions (i.e., a greater tendency for dissolution and regrowth to occur).

The phenomena of composition latching in InGaAs matched to InP has been observed by Takeda and Sasaki [27]. As discussed in the previous section, if the strain energy is significant when compared to mixing energies it can dominate the growth process and the layer will try to minimize the energy of the system by growing as a solid composition which is close to that matched to InP.

3.1.4. Doping

In this section both intentional and unintentional doping will be considered. To produce high-quality InGaAsP for microwave and photodetector applications where high mobility is paramount, the background impurity level in the crystal has to be reduced as far as possible. On the other hand, optical emitters such as double heterostructure lasers often require very high doping levels to provide a high level of carrier injection and to minimize contact resistance.

Considering first the background impurities; greater difficulty has been experienced in growing epitaxial layers by LPE from In-rich melts with background impurity levels comparable to GaAs grown from Ga solutions. The possibility of Si contamination being responsible has been widely discussed in the literature. Hicks and Greene [54] recognized the effect of Si contamination of the Ga solution from the SiO_2 growth tube during the growth of high-purity GaAs. The thermodynamic analysis contained in [54] was applied to InP LPE growth [55, 56]. The reaction can be described by

$$SiO_2(s) + H_2(g) \rightleftarrows SiO(g) + H_2O(g); \quad (16)$$

$$SiO(g) \rightleftarrows SiO(l); \text{ and} \quad (17)$$

$$SiO(l) + H_2(g) \rightleftarrows Si(l) + H_2O(g), \quad (18)$$

where $SiO_2(s)$ comes from the silica furnace tube, $H_2(g)$ is the growth atmosphere and Si(l) is the Si dissolved in the In-rich solution. The equilibrium constant, K, is given by

$$K = \frac{[Si]\,[H_2O]^2}{[H_2]^2[SiO_2]} \quad (19)$$

for the net reaction of Reactions 16 to 18, i.e.,

$$SiO_2(s) + 2H_2(g) \rightleftarrows Si(l) + 2H_2O(g). \quad (20)$$

Since the hydrogen and silica are nearly in their standard states,

$$[H_2] = [SiO_2] = 1 \quad (21)$$

and

$$K = [Si]\,[H_2O]^2. \quad (22)$$

The equilibrium constant is given by [56]

$$\log K = \frac{-2.65 \times 10^4}{T} + 5.65. \quad (23)$$

Since K is a constant for a given temperature, Equation 22 predicts that increasing the concentration of H_2O in the growth atmosphere will reduce the equilibrium Si concentration in the solution. At the same time, increasing the growth or bake-out temperature will increase the equilibrium Si concentration in the solution for a fixed amount of water vapour. This analysis then indicates the best procedures to be adopted to obtain minimum Si contamination of the melt. This problem of Si contamination is worse for InP since a distribution coefficient of about 30 has been measured [57] and since Si appears to act always as a donor in LPE InP, unlike the case of GaAs.

Attempts have been made recently by Groves and Plonko [58] to improve the purity of

$In_{0.8}Ga_{0.2}As_{0.5}P_{0.5}$ by intentionally adding trace amounts of H_2O to the growth ambient as predicted by the chemical analysis for InP. With the addition of 0.5 ppm H_2O to the ambient gas and for bake-out times of about 65 h, background levels of $1.3 \times 10^{15}\,cm^{-3}$ were achieved. This compares with layers from unbaked solutions having a carrier concentration of about $5 \times 10^{19}\,cm^{-3}$. The reduction was attributed directly to the presence of the water vapour driving Reaction 20 further to the left-hand side. Using PH_3 as a source of P for the solution also produced a lowering of impurities, but this was argued to be due to water vapour introduced from the source of PH_3. Greene *et al.* [59] obtained carrier concentrations in the low $10^{16}\,cm^{-3}$ range without any pre-bake of the growth solution and low $10^{15}\,cm^{-3}$ range when the solutions were baked for 10 h in an atmosphere of an estimated few parts per million H_2O in H_2. Their results covered the whole composition range of InGaAsP lattice-matched to InP. Baking of In without the other source materials led to no improvement in purity which seemed to indicate that contamination arose from the solute. A very recent publication by Oliver and Eastman [60] obtained background levels in the $10^{14}\,cm^{-3}$ range for GaInAs matched to InP by utilising a two-stage baking scheme designed to purge volatile impurities at high temperature before baking at the growth temperature to achieve a low equilibrium concentration of silicon in the solution.

Because of the large time constants in equilibrating the Si concentration in the In solution (of the order of hundreds of hours) and because of the difficulty in measuring water-vapour content at the low ppm and sub-ppm levels, reproducible attainment of low background levels in this quaternary system by LPE remains difficult. In addition, chemical analysis of these low levels of Si is not easy and the importance of other possible contaminants, such as sulphur, remains an uncertainty.

Considering intentional doping, it is a requirement of most devices to have rapid doping transitions or p–n junctions, the fabrication of which requires a knowledge of the distribution coefficients of the dopants. Several studies have been reported of doping in the system under review [35, 61–64]. Doping of the quaternary with composition $y \simeq 0.35$ was studied using Sn, Te and Zn [61]. Fig. 7 shows the curves of carrier density against fraction of dopant in the growth solution (solid curves). Feng *et al.* [61] also studied the effect

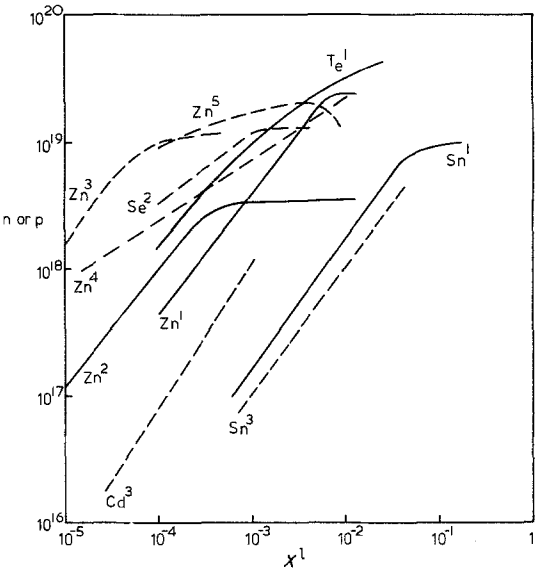

Figure 7 Variation of net carrier concentration against atom fraction in growth solution for various dopants. Lines are best-fits to the experimental points. (1) InGaAsP ($\lambda = 1.5\,\mu m$) [61]; (2) InGaAsP ($\lambda = 1.19\,\mu m$) [62]; (3) $In_{0.53}Ga_{0.47}As$ [63]; (4) $In_{0.53}Ga_{0.47}As$ [64]; (5) $In_{0.53}Ga_{0.47}As$ [35].

of added dopants on the change of quaternary composition grown from the same melt composition. It was found that in the case of Sn, Te and Zn, significant departures from the expected layer composition (for the case of no doping) were observed for melt fractions exceeding 10%, 1% and 1%, respectively. In these cases composition changes were observed through lattice parameter mismatches ($\Delta a/a$) of about 0.15, −0.1 and −0.2%, respectively. These effects could have serious consequences regarding surface morphology in highly-doped structures such as those required for double-heterostructure lasers. A dependence of Zn incorporation in InGaAsP on crystallographic orientation has been reported by Antypas and Shen [62].

Greater emphasis has been placed on studies of doping in the ternary InGaAs matched to InP which reflects the opinion that this is perhaps the most important composition of the quaternary, certainly as far as microwave or photodetector devices are concerned. Fig. 7 also shows curves for InGaAs (broken curves) for a wide range of dopant species. The lines are those drawn through experimental points. There is, in general, poor agreement between the curves, even for growth at similar temperatures. The main points to note from Fig. 7

are

(a) for highest doping levels, Te and Zn should be used for n-type and p-type, respectively; and

(b) Cd and Sn would form the easiest species to use for critical dopant control at low levels.

The use of Zn and Cd as dopants in InP to grow p–n junctions has indicated problems with high diffusion coefficients resulting in displaced p–n junctions with graded interfaces [65, 66]. These effects were partly due to the highly volatile nature of the dopants in the growth solution and partly due to high diffusion coefficients resulting in unwanted diffusion of the acceptors away from the metallurgical interface. The use of solution covers to prevent contamination of neighbouring melts and by growing at minimum temperatures for minimum time these effects could be successfully reduced [66]. Displaced p–n junctions have been observed in InP–InGaAsP double-heterostructure (DH) lasers [67] when using Zn as an acceptor. Taking the above mentioned precautions, correctly placed junctions were produced which led to improvements in efficiency of the lasers. It is evident therefore that great care should be taken when choosing the growth conditions of p–n junctions in the quaternary when Cd or Zn are used.

3.2. Vapour phase epitaxy

Because of practical difficulties, the use of vapour phase epitaxy (VPE) for growth of InGaAsP has been less popular than LPE. One of the main problems is due to the increased complexity of a four-component vapour which demands very precise control of partial pressures to enable correctly lattice-matched layers to be grown. The applications for VPE are similar to those of LPE grown layers but VPE has the added advantage that, in principle, large-area slices can be grown with a minimum of morphological defects.

There are two main VPE techniques suitable for the growth of InGaAsP: the so-called hydride system and the so-called metal–organic chemical vapour deposition (MOCVD) system. The hydride system can be described best by

$$\mathrm{III(l) + HCl(g) \rightarrow IIICl(g) + \tfrac{1}{2}H_2(g)} \quad (24)$$

$$\mathrm{4VH_3(g) \rightarrow V_4 + 6H_2(g)} \quad (25)$$

$$\mathrm{3IIICl(g) + \tfrac{1}{2}V_4(g) \rightarrow 2IIIV(s) + IIICl_3(g)}, \quad (26)$$

where III and V represent the Group three and Group five components, respectively. A schematic drawing of the vapour deposition system is shown in Fig. 8. Fig. 8 shows a system which would be capable of growing InGaAsP. The HCl flows over the free-Ga and In metal to form GaCl and InCl which is volatile (Reaction 24), AsH_3 and PH_3 diluted in purified H_2 is fed directly with the Group III chlorides. The vapours break down to the four constituents of the quaternary at the hot substrate surface and an epitaxial layer is grown (Reaction 25). Gas flows are regulated precisely using mass flow controllers. Dopant gases can be introduced at any point in the carrier gas flow. This technique has been successfully used to grow $In_{1-x}Ga_xAs_yP_{1-y}$ lattice-matched to InP [68]. In this case the mole fractions of the Group III and Group V materials in order to obtain lattice-matched layers were established. It has been shown that a lattice mismatch of about 0.1% could be tolerated before the surface of the layer became unsuitable for device fabrication. Double heterostructure InGaAsP–InP lasers have been success-

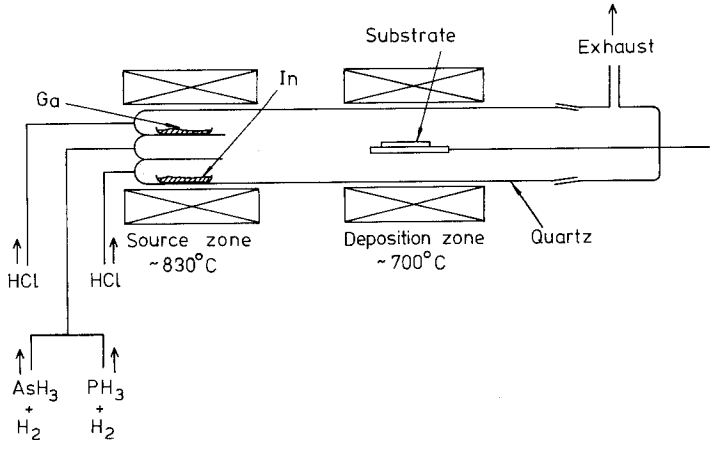

Figure 8 Diagramatic representation of the basic hydride VPE system capable of growing InGaAsP.

fully grown by this method [69] but no details of the growth conditions were published.

This system has also been used to grow InGaAsP on InP [70–72]. Kanbe *et al.* [72] studied the effects on temperature and substrate orientation on the growth conditions and found that different flows were required to be set up for (111) and (100) orientation InP substrates in order to obtain lattice matching. It was also found that the growth rate increased with increasing growth temperature for (100) and (111)B but that for (111)A orientation the temperature dependence was reversed. In addition, increased growth rate led to a reduction in background carrier level with a corresponding increase in mobility. Carrier levels, n, of $8 \times 10^{15}\,cm^{-3}$ with a mobility of $5500\,cm^2V^{-1}sec^{-1}$ were recorded. A development using a sliding silica boat to protect the InP substrate from thermal damage, has been incorporated [71] and a room-temperature mobility of $10050\,cm^2V^{-1}sec^{-1}$ at n of about $1 \times 10^{15}\,cm^{-3}$ was achieved. This system also resulted in a decrease in dark current in photodiodes made from this material.

There are some disadvantages associated with the hydride process just described, not the least of which is the inability to transport aluminium in the form of a mono-chloride. The MOCVD system has been developed in recent years and has the ability to transport all the reactants, including dopants, in a convenient vapour form. The basic reaction for this system is an irreversible pyrolysis which occurs on a heated substrate and can be described by

$$III(Alkyl)_3 + VH_3 \xrightarrow{heat} IIIV + 3\ Alkyl\ H, \quad (27)$$

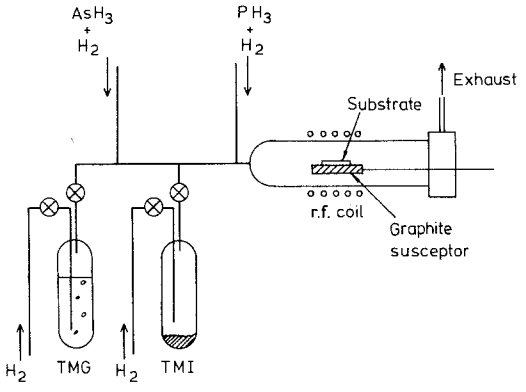

Figure 9 Schematic representation of the MOVPE system capable of growing InGaAsP.

where the first term is the Group III metal (ethyl or methyl) alkyl; a volatile hydrocarbon (the fourth term) is carried away to the exhaust. Fig. 9 shows the basic growth set-up. The alkyls are all liquid except for trimethyl indium (TMI) which is a solid at room temperature. The alkyl is picked up by a carrier H_2 gas which is bubbled through the liquid alkyl held at a constant temperature. In the case of TMI there is sufficient vapour pressure to load the carrier gas which passes over the solid. The alkyl vapours are mixed with the hydrides before passing over the substrate on a radio-frequency (r.f.) heated susceptor. The usefulness of the MOCVD system has been demonstrated by growing GaAs and GaAlAs for microwave devices and lasers. The growth of the phosphorus compounds have, however, proved more difficult due to the formation of a stable addition compound between PH_3 and the In alkyl. This polymer compound tends to form a powdery deposit which can block lines and make growth impossible. Duchemin *et al.* [73] have solved this problem by growing under low pressure (about 100 mbar) and also pyrolyzing the PH_3 before it comes into contact with the In alkyl. In view of this difficulty it would seem to be a good idea to keep the hydrides and metal alkyls separated until the last possible moment. Hirtz *et al.* [74] have used these techniques to grow InGaAsP–InP DH lasers. Diethyl Zn [$Zn(C_2H_5)_5$] and H_2S were used for p-type and n-type doping, respectively. The lasers exhibited electroluminescent efficiencies comparable to those grown by LPE in the same laboratory. $In_{0.53}Ga_{0.47}As$ on InP has also been grown in the same laboratory [75] and mobilities of $7740\,cm^2V^{-1}sec^{-1}$ were recorded for net carrier concentrations of $1 \times 10^{16}\,cm^{-3}$. An intentionally-doped layer of $n = 1.5 \times 10^{17}\,cm^{-3}$ gave a mobility of $6300\,cm^2V^{-1}sec^{-1}$ (approximately 50% higher than GaAs) which indicates the usefulness of this material for microwave applications.

A different solution to the problem of the formation of stable intermediate compounds has been presented by Renz *et al.* [76] for the growth of InP. These workers used an adduct of the type $(CH_3)_3\ In{-}P(CH_3)_3$ formed from triethyl indium and triethyl phosphorus. The adduct was in the form of a white powder at room temperature which had a sufficient vapour pressure to be transported in Ar and H_2 carrier gas. Other workers have used trimethyl arsenic (TMAS) instead of AsH_3 to grow InGaAs [77] and also avoided the

formation of addition compounds. Because of the pryophoric nature of the free metal alkyls and the extreme toxicity of the Group V hydrides, the use of relatively harmless adducts containing all the required components is very attractive indeed, and is sure to receive considerable attention in VPE studies in the near future.

3.3. Molecular beam epitaxy

Molecular beam epitaxy (MBE), whereby controlled molecular beams impinge on a heated substrate under ultra-high vacuum conditions, has been used in growing a variety of semiconductor thin films. The technique lends itself to precise doping and compositional control and, because of the slow growth rates (typically about $1\,\mu m\,h^{-1}$) attained with this method, extremely thin layers can be grown. Fig. 10 shows a typical layout of a stainless-steel MBE system with effusion sources sufficient for quaternary growth and doping. Extensive use of cryogenic panels in the chamber reduces the water-vapour and hydrocarbon content of the vacuum. For speed of operation and vacuum cleanliness, modern systems contain an air-lock for rapid sample loading. Analysing techniques such as Auger and mass spectroscopy and electron diffraction enable surface characterisation to be carried out *in situ*.

The ternary InGaAs lattice-matched to InP is the simplest alloy in the range under review to be grown by this method. Miller and McFee [78] were the first to grow this material by using a single effusion source of Ga–In in the correct ratio to grow lattice-matched material. Using a substrate temperature of 510° C, they were able to grow material with a solid Ga–In ratio to within 0.5% of that required for exact lattice matching. The rather high background doping levels of $n > 10^{17}\,cm^{-3}$ were attributed to impurities in the Ga–In source. The growth of double heterostructure InP–InGaAs–InP lasers was demonstrated. Asahi *et al.* [79] were able to grow this ternary from two separate sources of In and Ga and obtained compositional variations in the Group III sublattice over a 10 mm x 10 mm surface of ±1%. Carrier concentrations of $3 \times 10^{16}\,cm^{-3}$ with a room-temperature mobility of $6000\,cm^2\,V^{-1}\,sec^{-1}$ were obtained. Norris [80] illustrated that only over a limited substrate temperature range (400 to 430° C) could the solid composition be simply related to the incident flux levels. Mobilities of $6500\,cm^2\,V^{-1}\,sec^{-1}$ were achieved in this work.

Cho [81] has described the only reported growth of $In_{1-x}Ga_xAs_yP_{1-y}$ lattice-matched to InP by MBE. The problem with growing a phosphorus-bearing compound is the high vapour pressure of this element and the subsequent difficulty with the pumping system. In this work a single effusion cell was used for the In–Ga source and a mixture of polycrystalline GaAs and GaP with additional P was added to a second cell. The additional P allowed for the reduced sticking coefficient of this species. The Sn-doped $Ga_{0.12}In_{0.88}As_{0.23}P_{0.27}$ layer had a room-temperature mobility of $1650\,cm^2\,V^{-1}\,sec^{-1}$ at $n = 5 \times 10^{16}\,cm^{-3}$.

The properties of MBE growth have not yet been fully utilized in the InGaAsP quaternary system lattice-matched to InP. In particular, the slow growth rate and sharp interface transitions of this growth method lends itself to the growth of mobility-enhanced quantum-well structures. Also the use of both mechanical and oxide masks and the prospect of beam writing indicates that this technique will be very useful in realizing integrated circuits.

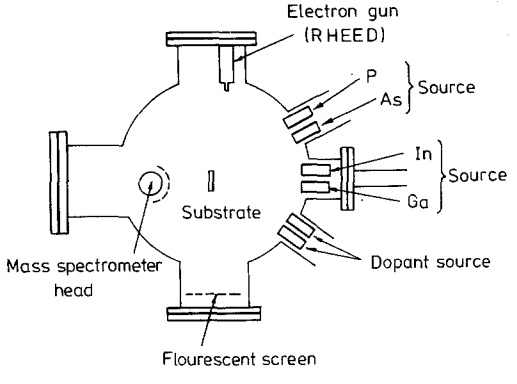

Figure 10 Schematic representation of the MBE apparatus.

4. Optical devices

4.1. Lasers and LED's

The rapid technological increase in InGaAsP sources for optical-fibre communication systems reflects the potential gains of this system over conventional coaxial cable systems. The present state of fibre technology [82] indicates two possible low-loss windows (Fig. 11) with minimum dispersion for silica-based fibres. The quaternary system is thus extremely useful in tailoring emission wavelengths of lasers to match current fibre technology. Most of the growth of lasers and LED's in this quaternary system is by LPE using multi-well

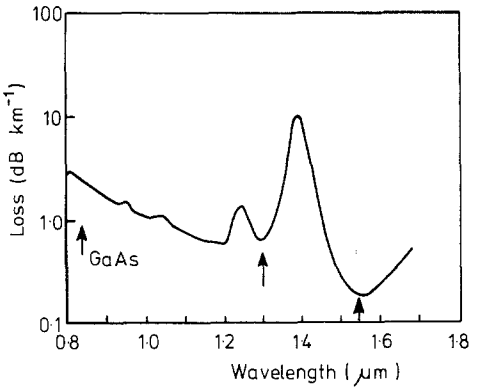

Figure 11 Spectral loss of silica-based optical fibres. Arrows indicate low-loss windows covered by InGaAsP and GaAs sources. Peaks are caused by OH vibrational absorption.

graphite sliding boats. The growth of the layers is usually initiated using a supercooled melt with various cooling rates, sometimes with solutions containing excess InP (two-phase technique) which somewhat alleviates the necessity of knowing the exact liquidus composition.

The operation of a double-heterostructure (DH) laser was first demonstrated by Bogatov *et al.* [83], using pulsed operation at 77 K. Subsequently, pulsed operation was obtained at room temperature [84, 85] using planar double heterojunction structures operating at 1.1 μm but with no attempt at optimizing the device dimensions. Pulsed threshold current densities of 10.4 kA cm^{-2} for an active layer thickness of 1.2 μm were reported in [84] and 2.8 kA cm^2 (0.6 μm) measured in [89]. Continuous wave (CW) operation at room temperature was first reported by Hsieh *et al.* [86]. These authors demonstrated the improvement in threshold current density which could be made by constructing stripe-geometry lasers whereby proton bombardment was used to create electrical isolation except for a 25 μm wide stripe (see Fig. 12).

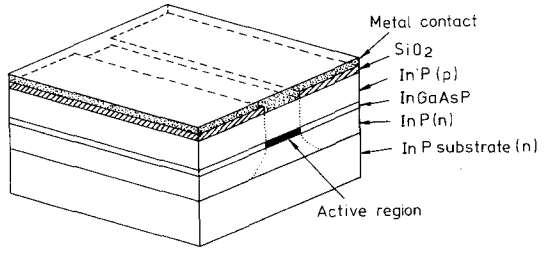

Figure 12 Schematic representation of InGaAsP–InP DH stripe laser. Dotted line shows the case of proton isolated stripe instead of SiO_2.

The lowest CW threshold value of about 4.7 kA cm^{-2} was recorded with an external quantum efficiency of about 10%. DH light-emitting diodes (LED's) were also fabricated for emission at 1.1 μm and a quantum efficiency of 4% was reported [87]. The work of Wright *et al.* [88] has demonstrated that many DH wafers can be grown from a single set of growth solutions. Even though melt depletion occurred for solutions at a fixed growth temperature and initial supersaturation, a change in growth rate of the layers was the only difference observed between the layers. In fact, DH layers showed good reproducibility of characteristics from wafter to wafer and from device to device. The carrier lifetime of an injection laser is important in determining the upper modulation speed limit. Itaya *et al.* [89] measured this parameter in three-layer InGaAsP–InP DH broad-area laser diodes operating at approximately 1.14 μm and their measured values of 20 to 30 nsec compares with 10 to 15 nsec for GaAs lasers, indicating comparable speed modulation performance. Shen *et al.* [90] demonstrated a 1500 h lifetime for a proton isolated stripe diode where the InP substrate had a dislocation density (5 × 10^5 cm^{-2}) larger than that normal for GaAs lasers which exhibit short lifetimes. This was a further encouraging sign for the InGaAsP laser source.

It was recognized that benefits could be had in moving to longer wavelengths to minimize fibre losses (Fig. 11) and a move to (100) orientation from (111) for ease of cleaving. CW operation lasers were made at 1.3 μm using a SiO_2 stripe geometry on (110) InP substrates. [91–93]. The stripes were defined by etching a 20 μm wide groove in a deposited SiO_2 film and then alloying evaporated metal contacts through this groove. A typical stripe geometry laser is shown schematically in Fig. 12. The stripe has the effect of confining the injection to a narrow region of the active layer directly below the gap in the SiO_2. An extra cap layer of InGaAsP was grown by Oe *et al.* [93] in an effort to reduce contact resistance since Zn can produce a higher doping level in the quaternary than InP. Stripe diodes from this work, however, exhibited a higher threshold current than broad-area diodes from the same wafer, indicating considerable current spreading in this structure. A CW threshold current density of 3.3 kA cm^{-2} was obtained for a 0.5 μm thick active layer and a lifetime of over 2000 h was demonstrated [93].

There are problems associated with growth

when extending the wavelength to greater than 1.3 μm. An InP solution cannot be in true thermodynamic equilibrium with a solid containing In–Ga–As–P (active layer) since the solid contains components not in the In–P solution. This means that there is a tendency for dissolution of the quaternary layer to occur into the In–P capping layer growth solution when the two are brought into contact. The situation is aggrevated by reducing the P content of the InGaAsP active layer to obtain longer wavelength operation. Nagai and Noguchi [18] solved this problem by growing an InGaAsP capping layer with a higher band-gap than the active layer, thus maintaining carrier confinement. This layer is normally referred to as the anti-meltback layer. The use of the quaternary capping layer had the added advantage of reducing the contact resistance. LED's and laser diodes were operated at 1.5 μm [18]. Arai *et al.* [94] described the two-phase supercooled technique for growing DH lasers and found them difficult to grow with wavelengths greater than 1.4 μm. This may have been due to dissolution of the active layer by the In–P capping layer solution rather than an inherent problem of growth of the InGaAsP active layer. They solved the problem by growing at a slightly lower temperature and obtained laser operation at 1.52 μm. Akiba and co-workers [95, 96] and Arai *et al.* [97] grew lasers at 1.67 μm which corresponds to an $In_{0.53}Ga_{0.47}As$ active layer and 1.5 μm, which corresponds to a minimum absorption in fibres. In one case [95], an InGaAsP capping layer was used to prevent meltback but a threshold current density of 15 kA cm^{-2} μm^{-1} was measured which is several times larger than lower wavelength lasers. In the other cases [95, 97] a thin InGaAsP anti-meltback layer was utilized before the InP confining layer was grown, which gave an improvement in threshold current to 8 to 11 kA cm^{-2} μm^{-1} [97]. This improvement was probably due to the increased confinement from the larger band-gap InP capping layer. A recent paper by Takahei *et al.* [98] describes growth of DH lasers at a low temperature (592° C) to eliminate meltback problems and shows that these lasers operated CW at 1.55 μm. Additional benefits of this growth temperature were the non-errosion of the InP substrates and the slow growth rate, enabling good control of active layer thickness.

A study of the dependence of threshold current on active layer thickness was made by Nahory and Pollack [99], using pulsed broad-area lasers operating at 1.23 μm. They found a normalized pulsed threshold current of 5 kA cm^{-2} per μm of active layer thickness for thicknesses in the range 1 to 0.4 μm with a minimum of 1.6 kA cm^2 at 0.2 μm. This only represented a limit for that particular material quality and device geometry. Arai *et al.* [94] have also studied this effect and obtained threshold current values of 4 to 5 kA cm^{-2} per μm with a lowest value of 1.2 kA cm^{-2} for a thickness of 0.32 μm. Fig. 13 shows plots of threshold current densities against active layer thickness with a theoretical best-fit curve [99] based on a model used successfully in GaAlAs–GaAs laser systems. The differences between the results of these authors are probably caused by final crystal quality and details of the device

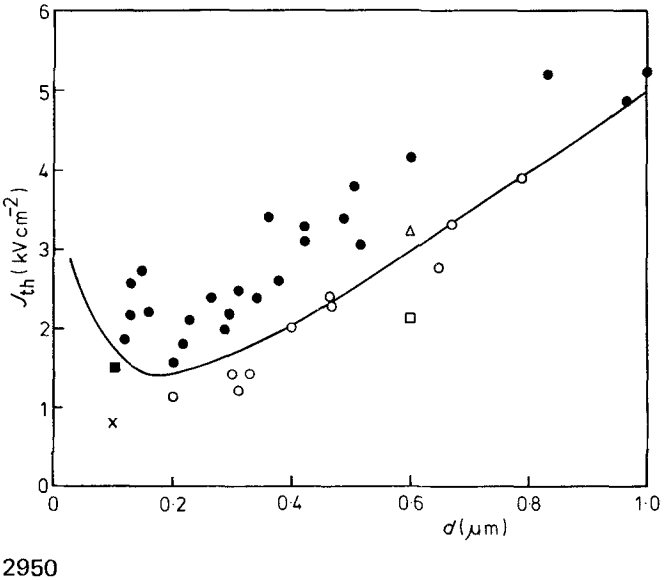

Figure 13 Measured and calculated threshold current density plotted against active layer thickness. —— theory [99]; • [99]; ○ [94]; □ [100]; × [102]; ■ VPE [69]; △ MBE [103].

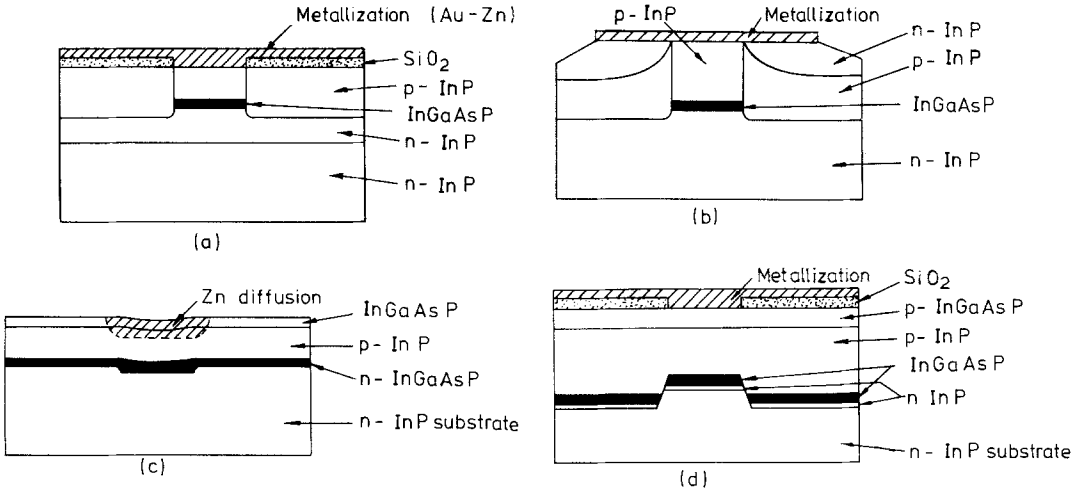

Figure 14 Various types of buried-heterostructure lasers operating at $\lambda \sim 1.3\,\mu m$. (a) Etch-back with SiO_2 current isolation; (b) etch-back with p–n junction isolation; (c) one-step growth on a grooved substrate; (d) one-step growth on a mesa-stripe substrate.

fabrication procedure. The threshold current density dependence on growth rate of the active layers [101] indicates that the lowest threshold could be obtained for the slowest growth rate or that closest to equilibrium. A value of $0.67\,kA\,cm^{-2}$ was recorded at an active layer thickness of $0.1\,\mu m$ for broad-area devices [102]. The higher values for step-cooled or two-phase solution growth could be due to composition grading or high defect concentrations introduced during rapid growth.

The importance of transverse mode stabilization in injection lasers has been demonstrated in the GaAlA–GaAs system. For efficient coupling to the optical fibre and to reduce the threshold current, a buried stripe structure is required in InGaAsP–InP lasers. Such a structure provides efficient carrier and optical confinement. Hsieh and Shen [102] fabricated buried-stripe DH InGaAsP–InP lasers. These two types of lasers are shown in Fig. 14 a and b. The fabrication procedure starts with the growth of a planar three-layer DH. The slice is then removed from the growth furnace and a SiO_2 stripe is formed on the top layer and selective etches such as HCl and $3H_2SO_4{:}H_2O{:}H_2O_2$ are used to remove the top InP layer and the InGaAsP layer, respectively, except for the area beneath the SiO_2 stripe. Subsequently a p–InP layer is regrown using the SiO_2 stripe as a mask, as in Fig. 14a, or successive p and n layers of InP are formed, as in Fig. 14b. Contact metallization is then introduced, as indicated in the diagram. The structure of Fig. 14b has the advantage of ensuring current confinement to the active region. These two structures have been similarly grown but in the latter case [104] etching down the lower InP layer was achieved by using an undersaturated In–P solution immediately prior to regrowth. This method probably has the advantage of reducing contamination but is much more difficult to control. Efficiencies of 10% and 14% per facet and CW threshold currents of 5.3 and $4.0\,kA\,cm^{-2}$ were achieved at 1.25 and $1.3\,\mu m$, respectively. A different approach to lateral guiding has been used by Doi *et al.* [105] using a one-step growth process on channels which are etched in a (1 1 0) n–InP substrate using $5H_2SO_4{:}H_2O{:}H_2O_2$ through an SiO_2 mask. An active layer of InGaAsP and a p–InP confining layer are then grown followed by an n–InGaAsP contacting layer. Zn is then selectively diffused down to the p–InP through an Al_2O_3 mask to form current-confining stripes. This device does not have full lateral confinement of the active layer by the confining InP and is shown schematically in Fig. 14c. Another one-step growth process has been discussed by Kishino and co-workers [106, 107] in which mesa-stripes are first etched on an InP substrate. Subsequent growth of the double heterostructure leaves a region of isolated active InGaAsP material on top of the mesa-stripes, as shown in Fig. 14d. Single longitudinal mode operation was obtained on these devices at up to 1.4 times the threshold current value. A very sophisticated buried heterostructure device operating at $1.3\,\mu m$ has been described recently by Murotani *et al.* [108]. With-

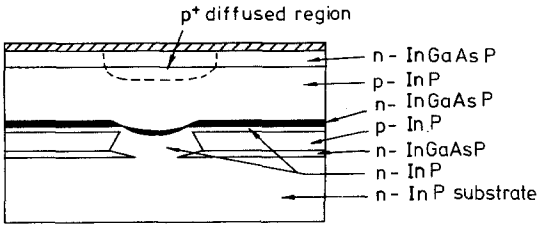

Figure 15 End view of a buried-cresent laser structure [107].

out the need for an anti-meltback layer, n–InGaAsP, p–InP and n–InGaAsP layers are sequentially grown and, using preferential etches, a dove-tail channel is etched down to the bottom quaternary layer. Subsequently, a saturated In–P solution for the growth of the first InP layer of the second-stage growth is used to etch back the quaternary layers at the surface and bottom of channel. The sequence of further grown layers is shown in Fig. 15. This etch-and-fill method has current-confining reverse-biased p–n junctions on either side of the active layer. Single-mode operation was obtained up to two times the threshold current. A very recent paper from the same laboratories [109] has reported the stabilization of the first-order transverse mode by restricting the width and thickness of the active region to below that required for higher-order cut-off.

Further refinements have been made to the basic buried-heterostructure concept and the wavelength extended to the important 1.55 to 1.6 μm region [110, 111]. The work in [110, 111] has made use of an InGaAsP anti-meltback layer over the active layer together with an InGaAsP contact layer; otherwise the structure is similar to that in Fig. 14b. Zn was diffused in the stripe area before the metallization was put down. In order to improve growth on the sides of the chemically-etched mesa-stripes, a slight *in situ* etch-back (0.5 μm), before subsequent growth of the InP blocking layers, was employed. Fundamental transverse mode operation was obtained up to three times the threshold current for a stripe width of 3 to 5 μm. The anti-meltback layer, although of higher band-gap than the active layer, is no substitute for InP as a confining layer. Consequently the low-temperature growth techniques developed in [98] were used to produce a buried heterostructure operating at 1.55 μm where the active layer was completely surrounded by InP [112]. The structure is similar to Fig. 14b. Takahashi *et al.* [113] have grown buried-heterostructure lasers at 1.55 μm on a channelled substrate without the need for either an anti-meltback layer or low temperature growth. The top InP-confining layer was grown from a solution supersaturated to greater than 15° C to suppress the active layer dissolution. Such large amounts of supercooling may lead to difficulties, however, with non-reproducible growth.

Conventional DH lasers with Fabrey–Perot resonators, although they can operate in single longitudinal mode under steady-state conditions, tend to revert to multi-mode operation under fast-pulse conditions. DH lasers have been fabricated with integrated distributed Bragg reflectors [110, 114, 115] which exhibit single-mode operation even at very high modulation rates. This reduces pulse broadening due to optical-fibre material dispersion. The active layer of the laser is coupled to a low-loss output guide of InGaAsP of a slightly lower band-gap wavelength in order to reduce absorption. This guide has corrugations formed on it to provide the distributed Bragg reflector which acts as a wavelength selector for single-mode operation. Operation of these devices at 1.3 μm [110, 115] and 1.5 to 1.6 μm [114] has been demonstrated and stable single longitudinal mode oscillation achieved, even at rise times of 300 psec. Spectral broadening due to carrier injection was eliminated.

All of the laser structures so far considered were grown by the well-tried LPE technique. DH lasers have been successfully grown by the hydride–chloride method [69] with a pulsed threshold of 1.5 to 2.5 kA cm^{-2} and quantum efficiencies of 50% operating at 1.25 μm. This performance compares very favourably with LPE lasers. The MOCVD grown lasers exhibited a threshold current denstiy of 5.9 kA cm^{-2} at 1.15 μm [74] but improvements in this are expected by optimizing the active layer growth conditions. Molecular beam epitaxy (MBE) has also been used to grow DH InGaAs–InP lasers operating at 1.65 μm [103]. These layers were grown using a premixed In–Ga single source to obtain composition uniformity. Difficulties were experienced in doping the InP with p-type dopant in the MBE set-up and also the residual carrier concentration in the active layer was rather high at around 2×10^{18} cm^{-3} (unintentionally doped). Nevertheless, threshold currents as low as 3.2 kA cm^{-2} for a 0.6 μm thick active layer were achieved but the

low quantum efficiencies (7 to 9%) were thought to be due to free carrier absorption from the highly-doped active layer and also interfacial states due to non-abrupt transitions.

A major problem with the InGaAsP system for lasers is the sharply increasing threshold current density and decreasing quantum efficiency with increasing temperature at temperatures above 250 K. The dependence of threshold current, J_{th}, on temperature is approximated by

$$J_{th}(T) = J_0 \exp(T/T_0), \qquad (28)$$

where T_0 is the temperature parameter and J_0 is the current extrapolated to 0 K. For temperatures less than 250 K, T_0 is typically between 100 and 150 K but T_0 is about 60 K for $T > 250$ K [93, 116]. This transition at 250 K is not observed in the GaAlAs–GaAs laser system. This small value of T_0 at around room temperature suggests that problems will occur in controlling laser output at elevated temperatures. Attempts at explaining these effects first implicated leakage current from the active layer into the InP confining layers [117]. This explanation was disputed, however, by showing that the threshold current density was independent of lasing wavelength [116, 118] and also by the lack of photoluminescence from the confining layers [119]. Only for $\lambda < 1.2\,\mu$m was carrier leakage shown to be the dominant loss mechanism [117]. The changes in heterobarrier energy differences at the different wavelengths would be expected to exhibit different leakage properties. The temperature dependence of carrier lifetime and radiative efficiency have been studied [119] and both show a discontinuity at a temperature similar to that of the threshold current. An additional non-radiative recombination centre was proposed as the mechanism for reducing the lifetime and some agreement with this picture has been obtained [118]. The possibility of band-to-band Auger recombination being partly responsible for the observed effects was also discussed [119]. More recently Adams *et al.* [120] have put forward a theory which describes the temperature variation of the absorption coefficient in terms of transitions from the split-off band to the heavy hole band and also to an acceptor level. The temperature variation of these two contributing mechanisms enables the quantum efficiency to be calculated as well as the threshold current density. The trend, with temperature, of these two quantities can be explained with this model although the non-radiative recombination mechanism may still be playing a part.

4.2 Photodetectors

Photodetectors are required in optical communication applications which will receive signals emitted from the sources discussed in the previous section. The traditional Si detectors will not respond beyond about 1.1 μm and Ge detectors suffer from large noise currents, partly due to the narrow band-gap. For the wavelengths being considered for optical communications systems, detectors are required which will operate out to 1.67 μm. These can be made from the same materials as the diode sources. The main features required of these photodiodes are high quantum efficiency and fast response time together with low noise characteristics. Fig. 16 shows a typical heterojunction photodiode structure where the incident radiation passes through the transparent InP top layer to interact with the InGaAsP layer to produce electron–hole pairs in the depletion region. The reverse bias can be increased to such a point where avalanche multiplication occurs and internal gain is obtained.

Photodiode detectors have been fabricated using the InGaAsP–InP system which can be tailored to respond in the wavelength, λ, range $0.9 < \lambda < 1.7\,\mu$m depending on window and absorption layer compositions, see, for example, [121]. External quantum efficiencies of between 50 and 70% are obtainable. This figure is limited by reflection and recombination effects at the surface or heterojunction interface, especially if absorption takes place in the top layer which then relies on diffusion of the carriers to reach the depletion region as in homojunction devices [24]. Photodiode detectors can also be constructed which are capable of detecting and de-multiplexing signals in two wavelength bands [122]. Two InGaAsP absorbing layers are formed in tandem on a single device with the higher band-gap layer facing the incident light to provide simultaneous detection of two different wavelengths. Apart from carrier transport properties (diffusion and drift), the response time of a photodetector can be limited by the resistance–capacitance (RC) time constant of the detection circuit. For this reason PIN diodes have been constructed in which a long low dopant-level ($\sim 10^{15}\,\mathrm{cm}^{-3}$) InGaAsP region (absorbing layer) is completely depleted under normal bias conditions, giving rise to capacitances

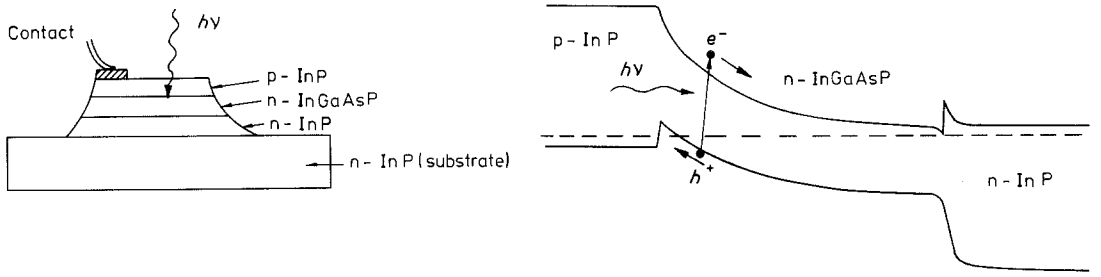

Figure 16 Heterojunction photodiode with n-InGaAsP as the absorbing layer and p-InP as the window layer.

of less than 1 pF at −20 V bias [123]. Similar results have been obtained with InGaAs absorbing layers in a PIN diode structure [124–126]. As had been pointed out previously [127], PIN photodiodes at wavelengths approaching 2 μm would have superior noise performance over avalanche photodiodes (APD's). Hence a PIN photodiode coupled to a low-noise FET amplifier was recognized as a possible match for Si ADP's. Smith *et al.* [128] mounted an InGaAs PIN photodiode hybrid-integrated with a GaAs MESFET preamplifier and obtained encouraging results even though the photodiode had a poor performance. Leheny *et al.* [129] demonstrated the first true integrated PIN–FET combination on a single slice of InGaAs. A current gain of approximately 30 was achieved.

Early attempts at fabricating APD's in the InGaAsP system resulted in large dark-current and low avalanche gain, see, for example, [130]. A small dark current is important since the signal output of an APD represents the difference between dark current and light current. The origin of the dark current has been variously attributed to microplasmas, surface effects and tunnelling. Nishida *et al.* [131] have constructed an APD where a diffused p–n junction is formed in the InP window layer rather than at the heterojunction. Fig. 17 shows the band structure of such a diode at high reverse bias. A large enough bias is applied such that the depletion region extends into the InGaAsP layer where electron–hole pairs are produced by incident light. The holes are injected into the avalanching region in the InP where multiplication occurs. Since only a small electric field is produced in the InGaAsP layer, large dark currents are avoided and the low-leakage and high-gain properties on InP are utilized. The donor concentration requirements to avoid Zener break-down in InGaAsP APD's have been calculated [132] since tunnelling has been shown to be an important source of leakage [133]. The use of guard-ring structures has also been successfully employed in reducing the leakage current [134]. The noise performance of an APD is determined by the ratio of electron-to-hole ionization rates, being lower for larger differences in the two rates, providing that the higher-rate carrier initiates the avalanche [24].

An alternative photodetector to APD's with internal gain is the heterojunction phototransistor. The principle of operation of this device can be

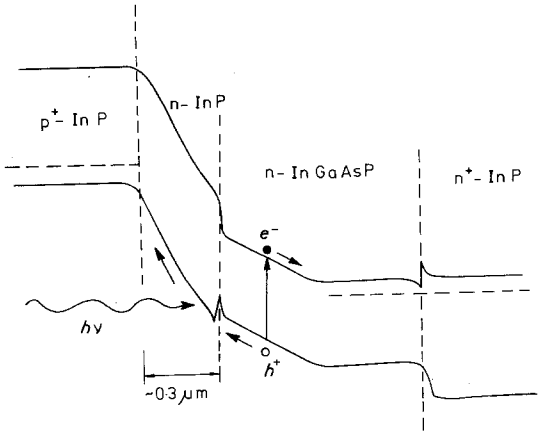

Figure 17 Band diagram of an InP–InGaAsP–InP avalanche photodiode where the p–n junction is located in the InP window layer and the depletion region extends to the InGaAsP absorbing layer. Holes are injected into the avalanche region from the InGaAsP layer.

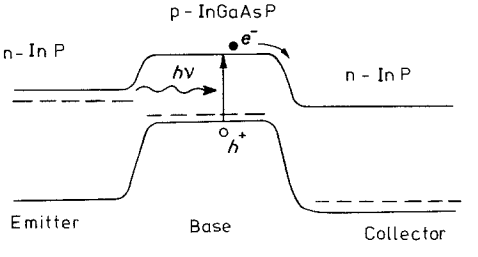

Figure 18 Band diagram of a heterojunction phototransistor where the base region absorbs the incident light.

seen from Fig. 18. The transistor has a floating base region and a reverse-biased base–collector junction. Incident light produces electron–hole pairs in the base region and the holes are trapped there while the electrons are collected. The trapped holes increase the forward bias on the emitter–base junction and amplification is achieved by the usual transistor action. The emitter–base heterojunction provides an injection efficiency close to unity since holes are prevented from entering the emitter. In this way, n–p–n phototransistors have been made and useful gains observed using InGaAs [135] or InGaAsP [136, 137] as the base material. The success of these devices indicates the possibilities of achieving integrated electro-optical circuits with sources, receivers, amplifiers and waveguides on one chip based on the InGaAsP–InP system.

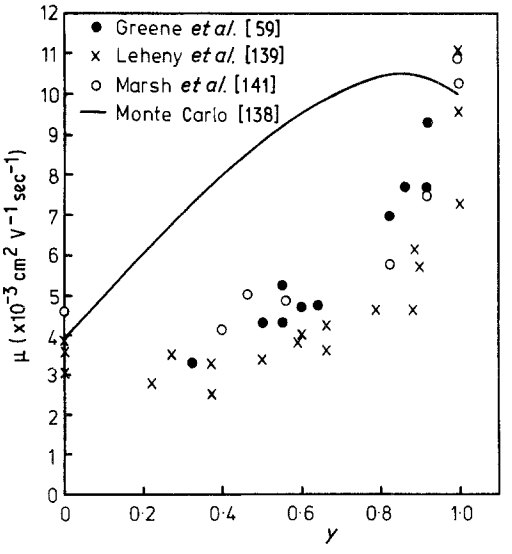

Figure 19 Low-field mobility of InGaAsP as a function of composition parameter y.

5. Non-optical applications

5.1. Transport properties

Initially, the great interest in InGaAsP lattice-matched to InP was almost exclusively in the field of optical devices. However, in 1977 Littlejohn *et al.* [138] performed Monte Carlo calculations which predicted mobilities and velocity–field characteristics which were superior to GaAs and InP for microwave device applications. These calculations caused a great deal of interest in this material for general high-speed applications but experimental observation [59, 139] did not agree with the calculated curves of low-field mobility across the composition range, lattice-matched to InP (see Fig. 19). This disagreement suggested that some of the material parameters used in the calculation [138] were not known with any great accuracy and attempts were made to fit Monte Carlo calculations to experimental mobility against temperature curves by varying material parameters such as total ionized impurity density and alloy scattering potential (measure of amount of alloy scattering) [140]. This exercise was of limited success, however, since calculations depended on the validity of the interpolation procedure for obtaining material parameters from the bonding binary compounds. Nevertheless, the important rôle of alloy scattering in limiting the low-field mobility was recognized. Estimates of the magnitude of alloy scattering have been made for electrons [141, 142] and holes [143] by calculating the individual contributions of mobility, μ, limited by the various scattering mechanisms and combining these using Matthiessens rule ($1/\mu_{\text{tot}} = \Sigma\, 1/\mu_i$) to match the total calculated mobility with that of the experimental μ–T curve. It is generally found that in order to get reasonable agreement with experimental results, an additional scattering factor with a temperature dependence of $\mu \propto T^{-1/2}$ has to be included. This temperature dependence is characteristic of either alloy scattering or space charge scattering. Assuming alloy scattering, the best-fit values of the alloy scattering potential, ΔU, were plotted as a function of the composition parameter, such that

$$\mu_{\text{alloy}} \propto \frac{1}{(\Delta U)^2 (kT)^{1/2} m^{*5/2}}, \qquad (29)$$

where k is the Boltzmann's constant, m^* is the effective mass and μ_{alloy} is the mobility limited by alloy scattering. This alloy scattering potential required to fit experiment is plotted in Fig. 20. There is a large scatter in the points which perhaps reflects the inaccuracies in the curve-fitting procedure, but a maximum of alloy scattering can be implied for $0.6 \lesssim y \lesssim 0.9$. This alloy scattering is thought to be the principal mechanism for the depression of the low-field mobility outlined in Fig. 19. The fact that alloy scattering dominates over space charge scattering has been tested for two compositions of $In_{1-x}Ga_xAs_yP_{1-y}$ ($y = 0.5$ and 0.91) by Adams *et al.* [144]. The different dependences of mobility on effective mass ($\mu_{\text{alloy}} \propto m^{*-5/2}$, $\mu_{\text{spacecharge}} \propto m^{*-1/2}$) were utilized by observing the mobility variation with pressure for

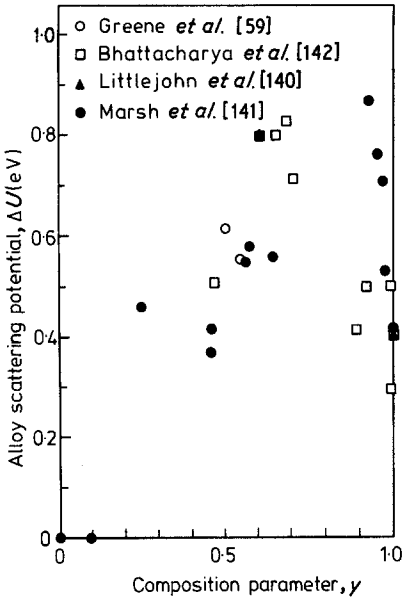

Figure 20 Alloy scattering potential as a function of composition parameter y.

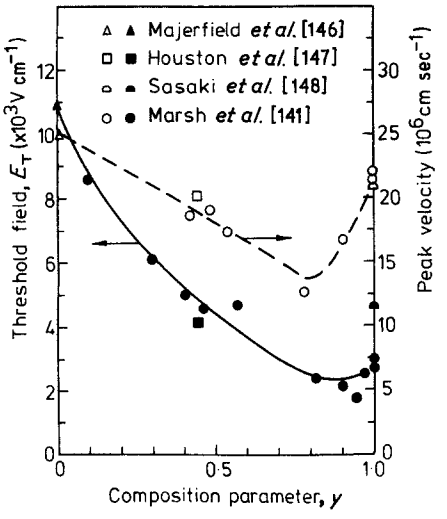

Figure 21 Peak velocity and threshold field plotted against composition parameter y. The peak velocity values are for samples with $N_D - N_A < 5 \times 10^{16}$ cm^{-3}.

the two samples. Since effective mass varies with pressure, the effective mass dependence was measured and compared with calculations based on alloy and space charge scattering. Alloy scattering was found to give the best fit to the experimental results.

The composition where the alloy scattering reaches a maximum may be a region close to solid immiscibility [47], as discussed in Section 3.1.2. Also, some difficulty is sometimes experienced in growing by LPE in this composition range. It may be that in this region, composition clustering takes place which would lead to enhanced alloy scattering. If this were the case, then ΔU would probably depend closely on growth parameters such as growth temperature. Pearsall [145] showed recently that the $T^{-1/2}$ temperature dependence of mobility was inadequate in describing the extra scattering mechanism in InGaAs. Clearly, a better insight into this scattering mechanism would help greatly in taking full advantage of the transport properties of this material system.

As well as low-field mobility, peak velocity and threshold field have been measured in this alloy system [141, 146–148] and are shown in Fig. 21. The dependence of these parameters on composition is closely linked to the band structure of InGaAsP and there is some suggestion that, in addition to inter-valley transfer, non-parabolicity in the lowest minimum may be significant in dictating the shape of the velocity–field characteristics [149]. Unfortunately, little is known about the detailed band structure in this alloy system.

The data of Figs 19 to 21 indicate that the ternary end-point, InGaAs, might be the most useful alloy in this system for microwave applications. Consequently, attention has been focussed on this ternary. Recently, room-temperature mobilities of 11 000 to 13 800 cm^2 V^{-1} sec^{-1} have been recorded [24, 59, 139] and these are the highest mobilities of any III–V semiconductor suitable for room-temperature operation. These results represent a big improvement over those obtained from InGaAs material grown earlier [26, 150]. From Fig. 21, it might be expected that transferred electron oscillation devices with improvements over GaAs or InP are possible. Such devices have been demonstrated [151] but little information on the operating properties have been given. However, estimates of threshold field and velocity are in agreement with values given in Fig. 21. Cappy *et al.* [152] have performed some computer calculations applicable to very short gate FET's and have shown that $In_{0.53}Ga_{0.47}As$ offers superior dynamic properties to InP or GaAs. Since the reduction of gate length in the quest for higher frequency operation makes use of transient transport properties of the material rather than steady-state properties, the ternary material would appear to be a very useful candidate for this application.

5.2 High-speed devices

The potential of InGaAsP, and especially InGaAs, lattice-matched to InP has been recognized for use in high-frequency microwave devices, high-speed logic and combinations of optical and switching devices integrated on one chip. The rapid advances in the field of optical sources and detectors has not been forthcoming with regard to high-speed devices. However, microwave devices have been made from this material in an attempt to take advantage of the high velocity characteristics. Morkoc *et al.* [153] constructed a microwave InGaAsP–InP microwave FET. A maximum direct current (d.c.) transconductance of about 10 msec for a device of width 200 μm and a gain of approximately 7 dB at 10 GHz has been obtained. Problems associated with high gate leakage currents were encountered due to the small barrier heights of the Schottky barriers made on this material (approximately 0.2 V for InGaAs). Leheny *et al.* [154] overcame this problem by using a Zn-diffused $In_{0.53}Ga_{0.47}As$ junction FET structure, but the diffusion process necessitated rather long gate lengths of 20 μm. Consequently, the full potential of the material was not realized. A different approach by Ohno *et al.* [155] was to grow an AlInAs–GaInAs–AlInAs double heterostructure MESFET using molecular beam epitaxy. The Al replaces the Ga to provide almost perfect lattice-matching and at the same time presents a surface to which a good Schottky barrier can be deposited. The double heterojunction interfaces result in good carrier confinement to the InGaAs layer. The d.c. transconductance for this device was 135 mS mm^{-1} for a 0.6 μm gate which compares favourably with 110 mS mm^{-1} for a good GaAs device of similar dimensions. The possibility of raising the effective barrier height for the InGaAsP system has been outlined by Morgan *et al.* [156] where a thin insulating layer is interposed between the metal and semiconductor. This structure shows some hysteresis in capacitance–voltage curves which is probably due to interfacial states at the oxide. These states could seriously affect the operation of MESFET's made using this structure and the problem of making good Schottky barriers indicates that developments in gate technology are important for this system.

6. Future prospects

The rapid advances in the InGaAsP quaternary system lattice-matched to InP has been mainly due to the interest shown in this material for optical sources. LPE growth technology has progressed sufficiently to enable sophisticated laser diodes to be constructed which will satisfy the requirements of long-wavelength optical-fibre communications systems. Single-mode operation at very low threshold currents has been established but problems of reliability and degradation mechanisms remain to be fully understood. In addition, further work is required to understand the mechanism of the large temperature sensitivity of the threshold current.

The use of this material for non-optical applications is at the early stages of development and it is perhaps in this area where the biggest advances are yet to be made. Microwave devices (Gunn, IMPATT's) often require low doping levels, and reproducible, transferrable methods of obtaining background carrier levels of about 10^{15} cm^{-3} would be useful. Investigations into the possibility of near-solid immiscibility occurring in the range of compositions under discussion would help clear up some puzzling aspects of growth in this region and may help in elucidating carrier scattering due to lattice disorder. In any case, a good physical picture of alloy scattering does not exist at present. Little is known about the detailed band structure of InGaAsP which is of fundamental importance in understanding the general transport properties, and particularly in understanding the transferred electron effect.

Future types of devices that are likely to achieve considerable attention are integrated circuits involving both optical and high-speed logic devices. Integrated optical circuits will contain sources (laser or LED), passive waveguides, modulators, couplers, switches and detectors all on one chip. This would be possible due to the versatile properties of the InGaAsP alloy range lattice-matched to InP (e.g., band-gap). High-speed integrated logic devices could combine the sensitive current control and short delay time of Gunn devices with the stable on–off operation of MESFET devices. Once the current growth problems associated with the MOCVD growth method have been overcome, the possibility of large-area epitaxial slices with a minimum of surface defects would greatly help in the production of integrated circuits. Growth techniques such as MBE and MOCVD offer the possibilities of selective-area growth which will ease the fabrication of integrated circuits.

In conclusion, the InGaAsP alloy system lattice-

matched to InP offers exciting device developments which will be superior even to the binary III–V alloys, GaAs and InP.

Acknowledgement

The author would like to express his gratitude to Professor P. N. Robson for his help and encouragement during the preparation of this paper.

References

1. R. E. NAHORY, M. A. POLLACK, W. D. JOHNSTON and R. L. BARNS, *Appl. Phys. Lett.* **33** (1978) 659.
2. R. L. MOON, G. A. ANTYPAS and L. W. JAMES, *J. Electronic Mater.* **3** (1974) 635.
3. K. NAKAJIMA, A. YAMAGUCHI, K. AKITA and T. KOTANI, *J. Appl. Phys.* **49** (1978) 5944.
4. Y. YAMAZOE, T. NISHINO, Y. HAMAKAWA and T. KARIYA, *Jap. J. Appl. Phys.* **19** (1980) 1473.
5. E. H. PEREA, E. E. MENDEZ and C. G. FONSTAD, *Appl. Phys. Lett.* **36** (1980) 978.
6. R. J. NICHOLAS, S. J. SESSIONS and J. C. PORTAL, *ibid.* **37** (1980) 178.
7. R. J. NICHOLAS, J. C. PORTAL, C. HOULBERY, P. PERRIER and T. P. PEARSALL, *ibid.* **34** (1979) 492.
8. J. B. RESTORFF, B. HOUSTON, R. S. ALLGAIER, M. A. LITTLEJOHN and S. B. PHATAK, *J. Appl. Phys.* **51** (1980) 2277.
9. H. BRENDECKE, H. L. STORMER and R. J. NELSON, *Appl. Phys. Lett.* **35** (1979) 772.
10. C. HERMANN and C. WEISBUCH, *Phys. Rev. B.* **15** (1977) 823.
11. G. A. ANTYPAS, R. L. MOON, L. W. JAMES, J. EDGECUMBE and R. L. BELL, Proceedings of the 1972 Symposium on GaAs, Boulder, Colorado, September 1972 (Institute of Physics, London, 1973) p. 48.
12. G. A. ANTYPAS and R. L. MOON, *J. Electrochem. Soc.* **120** (1973) 1574.
13. R. L. MOON and G. A. ANTYPAS, *J. Cryst. Growth* **19** (1973) 109.
14. G. A. ANTYPAS and J. EDGECUMBE, *ibid.* **34** (1976) 132.
15. K. NAKAJIMA, T. KUSONOKI, K. AKITA and T. KOTANI, *J. Electrochem. Soc.* **125** (1978) 123.
16. M. FENG, T. H. WINDHORN, M. M. TASHIMA and G. E. STILLMAN, *Appl. Phys. Lett.* **32** (1978) 758.
17. M. A. POLLACK, R. E. NAHORY, J. C. DE WINTER and A. A. BALLMAN, *ibid.* **33** (1978) 314.
18. H. NAGAI and Y. NOGUCHI, *ibid.* **32** (1978) 234.
19. K. SAKAI, S. AKIBA and T. YAMAMOTO, *Jap. J. Appl. Phys.* **16** (1977) 2043.
20. M. ILEGEMS and G. L. PEARSON, Proceedings of the 1968 Symposium on GaAs, Dallas, Texas, September 1968 (Institute of Physics and the Physical Society, London, 1969) p. 3.
21. J. J. HSIEH, M. C. FINN and J. A. ROSSI, Proceedings of the 1976 Conference on GaAs and Related Compounds, St. Louis, September 1976 (Institute of Physics, London, 1977) p. 37.
22. G. A. ANTYPAS and L. Y. L. SHEN, Proceedings of the 1976 Conference on GaAs and Related Compounds, St. Louis, 1976 (Institute of Physics, London, 1977) p. 26.
23. K. OE and K. SUGIYAMA, *Appl. Phys. Lett.* **33** (1978) 449.
24. T. P. PEARSALL, *IEEE J. Quant. Elect.* **QE-16** (1980) 709.
25. T. Y. WU and G. L. PEARSON, *J. Phys. Chem. Solids* **33** (1972) 409.
26. S. B. HYDER, G. A. ANTYPAS, J. S. ESCHER and P. E. GREGORY, *Appl. Phys. Lett.* **31** (1977) 551.
27. Y. TAKEDA and A. SASAKI, *J. Cryst. Growth* **45** (1978) 257.
28. Y. TAKEDA, A. SASAKI, Y. IMAMURA and T. TAKAGI, *J. Appl. Phys.* **47** (1976) 5405.
29. R. SANKARAN, R. L. MOON and G. A. ANTYPAS, *J. Cryst. Growth* **33** (1976) 271.
30. T. P. PEARSALL, R. BISARD, R. ANSEL and P. MERENDA, *Appl. Phys. Lett.* **32** (1978) 497.
31. G. A. ANTYPAS, Y. M. HOUNG, S. B. HYDER, J. S. ESCHER and P. E. GREGORY, *ibid.* **33** (1978) 463.
32. T. KOTANI, A. YAMAGUCHI, K. AKITA and S. NAKAI, *J. Cryst. Growth* **44** (1978) 543.
33. K. SAKAI, V. MATSUMSHIMA, S. AKIBA and T. YAMAMOTO, *Jap. J. Appl. Phys.* **18** (1979) 1009.
34. K. NAKAJIMA, T. TANAHASHI, K. AKITA, and T. YAMAOKA, *J. Appl. Phys.* **50** (1979) 4975.
35. J. L. BENCHIMOL, M. QUILLEC, C. LE CORNEC and G. LE ROUX, *Appl. Phys. Lett.* **36** (1980) 454.
36. R. SANKARAN, G. A. ANTYPAS, R. L. MOON, J. S. ESCHER and L. W. JAMES, *J. Vac. Sci. Technol.* **13** (1976) 932.
37. K. J. BACHMANN and J. L. SHAY, *Appl. Phys. Lett.* **32** (1978) 446.
38. T. P. PEARSALL and R. W. HOPSON, *J. Appl. Phys.* **48** (1977) 4407.
39. A. S. JORDAN and M. ILEGEMS, *J. Phys. Chem. Sol.* **36** (1975) 329.
40. A. S. JORDAN, *J. Electrochem. Soc.* (1972) 123.
41. G. B. STRINGFELLOW, *ibid.* **34** (1973) 1749.
42. *Idem, J. Cryst. Growth* **27** (1974) 21.
43. M. B. PANISH and M. ILEGEMS, "Progress in Solid State Chemistry" Vol. 7 (Pergamon Press, Oxford and New York, 1972) pp. 39–83.
44. S. M. BEDAIR, C. MORRISON, R. FANG and N. A. EL-MASRY, *J. Appl. Phys.* **51** (1980) 5413.
45. E. H. PEREA and G. FONSTAD, *ibid.* **51** (1980) 331.
46. E. H. PEREA and G. FONSTAD, *J. Electrochem. Soc.* **127** (1980) 313.
47. B. DE CREMOUX, P. HIRTZ and J. RICCIARDI, Proceedings of the 1980 Symposium on GaAs and Related Compounds, Vienna, September 1980 (Institute of Physics, London), to be published.
48. B. DE CREMOUX, Proceedings of the 1978 Sym-

posium on GaAs and Related Compounds, St. Louis, September 1978 (Institute of Physics, London, 1979) p. 52.
49. R. E. NAHORY, M. A. POLLACK, E. D. BEEBE, J. C. DE WINTER and M. ILEGEMS, *J. Electrochem. Soc.* **125** (1978) 1053.
50. M. FENG, M. M. TASHIMA, T. H. WINDHORN and G. E. STILLMAN, *Appl. Phys. Lett.* **33** (1978) 533.
51. R. BISARO, P. MERENDA and T. P. PEARSALL, *ibid.* **34** (1979) 100.
52. K. NAKAJIMA, S. KOMIYA, K. AKITA, T. YAMOAKA and O. RYUZAN, *J. Electrochem. Soc.* **127** (1980) 1568.
53. M. FENG, L. W. COOK, M. M. TASHIMA, G. E. STILLMAN and R. J. BLATTNER, *Appl. Phys. Lett.* **34** (1979) 697.
54. H. G. B. HICKS and P. D. GREENE, Proceedings of the 3rd International Symposium of GaAs, Aachen, October 1970 (Institute of Physics, London, 1971) p. 92.
55. K. T. IP, L. F. EASTMAN and V. L. WRICK, *Elect. Lett.* **13** (1977) 682.
56. V. L. WRICK, K. T. IP and L. F. EASTMAN, *J. Elect. Mater.* 7 (1978) 253.
57. G. G. BAUMANN, K. W. BENZ and M. H. PILKUHN, *J. Electrochem. Soc.* **123** (1976) 1232.
58. S. H. GROVES and M. C. PLONKO, Proceedings of the 1978 Symposium on GaAs and Related Compounds, St. Louis, September 1978 (Institute of Physics, London, 1979) p. 71.
59. P. D. GREENE, S. A. WHEELER, A. R. ADAMS, A. N. EL-SABBAHY and C. N. AHMAD, *Appl. Phys. Lett.* **35** (1979) 78.
60. J. D. OLIVER and L. F. EASTMAN, *J. Elect. Mater.* **9** (1980) 693.
61. M. FENG, M. M. TASHIMA, L. W. COOKE, R. A. MILANO and G. E. STILLMAN, *Appl. Phys. Lett.* **34** (1979) 91.
62. G. A. ANTYPAS and L. Y. L. SHEN, Proceedings of the 1976 International Symposium on GaAs and Related Compounds, St. Louis, September 1976 (Institute of Physics, London, 1977) p. 96.
63. T. P. PEARSALL, G. BEUCHET, J. P. HIRTZ, N. VISENTIN and M. BONNET, Proceedings of the 1980 Conference on GaAs and Related Compounds, Vienna, September 1980 (Institute of Physics, London), to be published.
64. Y. TAKEDA, M. KUZUHARA and A. SASAKI, *Jap. J. Appl. Phys.* **19** (1980) 899.
65. O. WADA, A. MAJERFELD and P. N. ROBSON, *J. Electrochem. Soc.* **127** (1980) 2278.
66. I. UMEBU and P. N. ROBSON, *J. Cryst. Growth* **53** (1981) 292.
67. J. J. COLEMAN and F. R. NASH, *Elect. Lett.* **14** (1978) 559.
68. S. B. HYDER, R. R. SAXENA and C. C. HOOPER, *Appl. Phys. Lett.* **34** (1979) 584.
69. G. H. OLSEN, C. J. NUESE and M. ETTENBERG, *ibid.* **34** (1979) 262.
70. H. NAGAI, *J. Appl. Phys.* **45** (1974) 3789.
71. N. SUSA, Y. YAMAUCHI, H. ANDO and H. KANBE, *Jap. J. Appl. Phys.* **19** (1979) L17.
72. H. KANBE, Y. YAMAUCHI and N. SUSA, *Appl. Phys. Lett.* **35** (1979) 603.
73. J. P. DUCHEMIN, M. BONNET, G. BEUCHET and F. FOELSCH, Proceedings of the 1978 Symposium on GaAs and Related Compounds, St. Louis, 1978, (Institute of Physics, London, 1979) p. 10.
74. J. P. HIRTZ, J. P. DUCHEMIN, P. HIRTZ, B. DE CREMOUX, T. PEARSALL and M. BONNET, *Elect. Lett.* **16** (1980) 275.
75. J. P. HIRTZ, J. P. LARIVAIN, J. P. DUCHEMIN, T. P. PEARSALL and M. BONNET, *ibid.* **16** (1980) 415.
76. H. RENZ, J. WEIDLEIN, K. W. BENZ and M. H. PILKUHN, *ibid.* **16** (1980) 228.
77. C. B. COOPER, M. J. LUDOWISE, V. AEBI and R. L. MOON, *ibid.* **16** (1980) 20.
78. B. I. MILLER and J. H. McFEE, *J. Electrochem. Soc.* **125** (1978) 1310.
79. H. ASAHI, H. OKAMOTO, M. IKEDA and Y. KAWAMURA, *Jap. J. Appl. Phys.* **18** (1979) 565.
80. M. T. NORRIS, *Appl. Phys. Lett.* **36** (1980) 833.
81. A. Y. CHO, *J. Vac. Sci. Technol.* **16** (1979) 275.
82. T. MIYA, Y. TERUNUMA, T. HOSAKA and T. MIYASHITA, *Elect. Lett.* **15** (1979) 106.
83. A. P. BOGATOV, L. M. DOLGINOV, L. V. DRUZHININA, P. G. ELISEEV, B. N. SVERDLOV and E. G. SHEVEHENKO, *Soviet J. Quant. Elect.* **4** (1975) 1281.
84. A. P. BOGATOV, L. M. DOLGINOV, P. G. ELISEEV, M. G. MIL'VIDSKY, B. N. SVERDLOV and E. G. SHEVCHENKU, *Soviet Phys. Semicond.* **9** (1976) 1282.
85. J. J. HSIEH, *Appl. Phys. Lett.* **28** (1976) 283.
86. J. J. HSIEH, J. A. ROSSI and J. P. DONNELLY, *ibid.* **28** (1976) 709.
87. T. P. PEARSALL, B. I. MILLER, R. J. CAPIK and K. T. BACHMANN, *ibid.* **28** (1976) 499.
88. P. D. WRIGHT, E. A. REZEK, N. HOLONYAK, G. E. STILLMAN, J. A. ROSSI and W. O. GROVES, *ibid.* **31** (1977) 40.
89. Y. ITAYA, Y. SUEMATSU and K. IGA, *Jap. J. Appl. Phys.* **16** (1977) 1057.
90. C. C. SHEN, J. J. HSIEH and T. A. LIND, *Appl. Phys. Lett.* **30** (1977) 353.
91. K. OE, S. ANDO and K. SUGIYAMA, *Jap. J. Appl. Phys.* **16** (1977) 1273.
92. T. YAMAMOTO, K. SAKAI, S. AKIBA, *ibid.* **16** (1977) 1699.
93. T. YAMAMOTO, K. SAKAI, S. AKIBA and Y. SUEMATSU, *IEEE J. Quant. Electr.* **QE-14** (1978) 95.
94. S. ARAI, V. ITAYA, Y. SUEMATSU, K. KISHINO and S. KATAYAMA, *Jap. J. Appl. Phys.* **17** (1978) 2067.
95. S. AKIBA, K. SAKAI and T. YAMAMOTO, *ibid.* **17** (1978) 1899.
96. S. AKIBA, K. SAKAI, Y. MATSUSHIMA and T. YAMAMOTO, *Elect. Lett.* **15** (1979) 606.
97. S. ARAI, Y. SUEMATSU and Y. ITAYA, *Jap. J. Appl. Phys.* **18** (1979) 709.
98. K. TAKAHEI, H. NAGAI and H. KAWAGUCHI,

Appl. Phys. Lett. **36** (1980) 309.
99. R. E. NAHORY and M. A. POLLACK, *Elect. Lett.* **14** (1978) 727.
100. G. D. HENSHALL and P. D. GREENE, *ibid.* **15** (1979) 621.
101. R. J. NELSON, *Appl. Phys. Lett.* **35** (1979) 654.
102. J. J. HSIEH and C. C. SHEN, *ibid.* **30** (1977) 429.
103. B. I. MILLER, H. H. McFEE, R. J. MARTIN and P. K. TIEN, *Appl. Phys. Lett.* **33** (1978) 44.
104. H. KANO, K. OE, S. ANDO and K. SUGIYAMA, *Jap. J. Appl. Phys.* **17** (1978) 1887.
105. A. DOI, N. CHINONE, K. AIKI and R. ITO, *Appl. Phys. Lett.* **34** (1979) 393.
106. K. KISHINO, Y. SUEMATSU and Y. ITAYA, *Elect. Lett.* **15** (1979) 134.
107. K. KISHINO, Y. SUEMATSU, U. TAKAHASHI T. TANBUN-EK and Y. ITAYA, *IEEE J. Quant. Elect.* **QE-16** (1980) 160.
108. T. MUROTANI, E. OOMURA, H. HIGUCHI, H. NAMIZAKI and W. SUSAKI, *Elect. Lett.* **16** (1980) 566.
109. E. OOMURA, H. HIGUCHI, R. HIRANO, H. NAMIZAKI, T. MUROTANI and W. SUSAKI, *Elect. Lett.* **17** (1981) 83.
110. Y. ITAYA, T. TANBUN-EK, K. KISHINO, S. ARAI and Y. SUEMATSU, *Jap. J. Appl. Phys.* **19** (1980) L141.
111. S. ARAI, M. ASADO, Y. SUEMATSU, S. ITAYA, T. TANBUN-EK and K. KISHINO, *Elect. Lett.* **16** (1980) 349.
112. H. NAGAI, Y. NOGUCHI, K. TAKAHEI, Y. TOYOSHIMA and G. IWANE, *Jap. J. Appl. Phys.* **19** (1980) L218.
113. S. TAKAHASHI, H. SAITO and G. IWANE, *Elect. Lett.* **16** (1980) 922.
114. K. UTAKA, K. KOBAYASHI, K. KISHINO and Y. SUEMATSU, *Elect. Lett.* **16** (1980) 455.
115. Y. SAKAKIBARA, K. FURUYA, K. UTAKA and Y. SUEMATSU. *ibid.* **16** (1980) 456.
116. S. ARAI and Y. SUEMATSU, *IEEE J. Quant. Elect.* **QE-16** (1980) 197.
117. M. ETTEMBERG, C. J. NEUSE and H. KRESSEL, *J. Appl. Phys.* **50** (1979) 2949.
118. R. E. NAHORY, M. A. POLLACK and J. C. DE WINTER, *Elect. Lett.* **15** (1979) 695.
119. Y. HORIKOSHI and Y. FURUKAWA, *Jap. J. Appl. Phys.* **18** (1979) 809.
120. A. R. ADAMS, M. ASADA, Y. SUEMATSU and S. ARAI, *Jap. J. Appl. Phys.* **19** (1980) L621.
121. M. A. WASHINGTON, R. E. NAHORY, M. A. POLLACK and E. D. BEEBE, *Appl. Phys. Lett.* **33** (1978) 854.
122. T. P. LEE, J. C. CAMPBELL, K. OGAWA, A. R. McCORMICK, A. G. DENTAI and C. A. BURRUS, *Elect. Lett.* **15** (1979) 388.
123. C. A. BURRUS, A. G. DENTAI and T. P. LEE, *ibid.* **15** (1979) 655.
124. R. F. LEHENY, R. E. NAHORY and M. A. POLLACK, *ibid.* **15** (1979) 713.
125. T. P. LEE, G. A. BURRUS, A. G. DENTAI and K. OGAWA, *ibid.* **16** (1980) 155.
126. F. CAPASSO, R. A. LOGAN, A. HUTCHINSON and D. D. MANCHON, *ibid.* **16** (1980) 893.
127. S. HATA, K. KATIYAMA and Y. MIZUSHIMA, *ibid.* **13** (1977) 668.
128. D. R. SMITH, R. C. HOOPER, K. AHMAD, D. JENKINS, A. W. MABBITT and R. NICKLIN, *ibid.* **16** (1980) 69.
129. R. F. LEHENY, R. E. NAHORY, M. A. POLLACK, A. A. BALLMAN, E. D. BEEBE, J. C. DE WINTER and R. J. MARTIN, *ibid.* **16** (1980) 353.
130. H. D. LAW, L. R. TOMASETTA and K. NAKANO, *Appl. Phys. Lett.* **33** (1978) 920.
131. K. NISHIDA, K. TAGUCHI and Y. MATSUMOTO, *ibid.* **35** (1979) 251.
132. Y. TAKANASHI, M. KAWASHIMA and Y. HORIKOSHI, *Jap. J. Appl. Phys.* **19** (1980) 693.
133. H. ANIDO, H. KANBE, M. ITO and T. KANEDA, *ibid.* **19** (1980) L277.
134. F. OSAKA, K. NAKAZIMA, T. KANEDA, T. SAKURAI and N. SUSA, *Elect. Lett.* **16** (1980) 716.
135. J. C. CAMPBELL, A. G. DENTAI, C. A. BURRUS and J. F. FERGUSON, *ibid.* **16** (1980) 713.
136. M. TOBE, Y. AMEMIYA, S. SAKAI and M. UMEMO, *Appl. Phys. Lett.* **37** (1980) 73.
137. P. D. WRIGHT, R. J. NELSON and T. CELLA, *ibid.* **37** (1980) 192.
138. M. A. LITTLEJOHN, J. R. HAUSER and T. H. GLISSON, *ibid.* **30** (1977) 242.
139. R. F. LEHENY, A. A. BALLMAN, J. C. DE WINTER, R. E. NAHORY and M. A. POLLACK, *J. Elect. Mater.* **9** (1980) 561.
140. M. A. LITTLEJOHN, R. A. SADLER, T. H. GLISSON and J. R. HAUSER, Proceedings of the 1978 Conference on GaAs and Related Compounds, St. Louis, September 1978 (Institute of Physics, London, 1979) p. 239.
141. J. H. MARSH, P. A. HOUSTON and P. N. ROBSON, Proceedings of the 1980 Conference on GaAs and Related Compounds, Vienna, September 1980 (Institute of Physics, London), to be published.
142. P. K. BHATTACHARYA, J. W. KU, S. J. T. OWEN, G. H. OLSEN and S. H. CHIAO, *IEEE J. Quant. Elect.*, **17** (1981) 150.
143. J. R. HAYES, A. R. ADAMS and P. D. GREENE, *Elect. Lett.* **16** (1980) 282.
144. A. R. ADAMS, H. L. TATHAM, J. R. HAYES, A. N. EL-SABBAHY and P. D. GREENE, *ibid.* **16** (1980) 560.
145. T. P. PEARSALL, *ibid.* **17** (1981) 169.
146. A. MAJERFELD, K. E. POTTER and P. N. ROBSON, *J. Appl. Phys.* **45** (1974) 3681.
147. B. HOUSTON, J. B. RESTORFF, R. S. ALLGAIER, J. R. BURKE, D. K. FERRY and G. A. ANTYPAS, *Sol. Stat. Elect.* **21** (1978) 91.
148. A. SASAKI, *Jap. J. Appl. Phys.* **16** (1977) 239.
149. J. R. HAUSER, T. H. GLISSON and M. A. LITTLEJOHN, *Sol. Stat. Elect.* **22** (1979) 487.
150. A. SASAKI, Y. TAKEDA, N. SHIKAGAWA and T. TAKAGI, *Jap. J. Appl. Phys.* **16** (1977) 239 (Supplement 16-1).
151. Y. TAKEDA, N. SHIKAGAWA and A. SASAKI, *Sol. Stat. Electr.* **23** (1980) 1003.
152. A. CAPPY, B. CARNEZ, R. FAUQUEMBERGUES,

G. SALMER and E. CONSTANT, *IEEE Trans. Elect. Dev.* **ED-27** (1980) 2158.
153. H. MORKOC, J. T. ANDREWS, Y. M. HOUNG, R. SANKARAN, S. G. BANDY and G. A. ANTYPAS, *Elect. Lett.* **14** (1978) 448.
154. R. F. LEHENY, R. E. NAHORY, M. A. POLLACK, A. A. BALLMAN, E. D. BEEBE, J. C. DEWINTER and R. J. MARTIN, *IEEE Elect. Dev. Let.* **EDL-1** (1980) 110.
155. H. OHNO, J. BARNARD, L. RATHBUN, C. E. C. WOOD and L. F. EASTMAN, Proceedings of the 1980 Conference on GaAs and Related Compounds, Vienna, September 1980 (Institute of Physics, London), to be published.
156. D. V. MORGAN, J. FREY and W. J. DEVLIN, *J. Electrochem. Soc.* **127** (1980) 1202.

Received 10 March and accepted 19 June 1981.